Air Force Institute of Technology
AFIT Scholar

Theses and Dissertations | Student Graduate Works

3-2006

Inertia Measurement and Dynamic Stability Analysis of a Radio-Controlled Joined-Wing Aircraft

William A. McClelland

Follow this and additional works at: https://scholar.afit.edu/etd

 Part of the Aerospace Engineering Commons, and the Mechanical Engineering Commons

Recommended Citation

McClelland, William A., "Inertia Measurement and Dynamic Stability Analysis of a Radio-Controlled Joined-Wing Aircraft" (2006). *Theses and Dissertations*. 3521.
https://scholar.afit.edu/etd/3521

This Thesis is brought to you for free and open access by the Student Graduate Works at AFIT Scholar. It has been accepted for inclusion in Theses and Dissertations by an authorized administrator of AFIT Scholar. For more information, please contact AFIT.ENWL.Repository@us.af.mil.

INERTIA MEASUREMENT AND DYNAMIC STABILITY ANALYSIS OF A RADIO-CONTROLLED JOINED-WING AIRCRAFT

William A. McClelland, Captain, USAF

AFIT/GA/ENY/06-M07

DEPARTMENT OF THE AIR FORCE
AIR UNIVERSITY

AIR FORCE INSTITUTE OF TECHNOLOGY

Wright-Patterson Air Force Base, Ohio

APPROVED FOR PUBLIC RELEASE; DISTRIBUTION UNLIMITED

The views expressed in this thesis are those of the author and do not reflect the official policy or position of the United States Air Force, Department of Defense, or the U.S. Government.

AFIT/GA/ENY/06-M07

INERTIA MEASUREMENT AND DYNAMIC STABILITY ANALYSIS OF A RADIO-CONTROLLED JOINED-WING AIRCRAFT

THESIS

Presented to the Faculty

Department of Aeronautical Engineering

Graduate School of Engineering and Management

Air Force Institute of Technology

Air University

Air Education and Training Command

In Partial Fulfillment of the Requirements for the

Degree of Master of Science in Aeronautical Engineering

William A. McClelland, BS

Captain, USAF

March 2006

APPROVED FOR PUBLIC RELEASE; DISTRIBUTION UNLIMITED

AFIT/GA/ENY/06-M07

INERTIA MEASUREMENT AND DYNAMIC STABILITY ANALYSIS OF A RADIO-CONTROLLED JOINED-WING AIRCRAFT

William A. McClelland, BS

Captain, USAF

Approved:

_____	_____
Robert Canfield (Chairman)	Date
_____	_____
Eric Stephen, Lt Col, USAF (Member)	Date
_____	_____
Donald Kunz (Member)	Date

AFIT/GA/ENY/06-M07

Abstract

Dynamic stability and stall during steady level turns were examined for VA-1, a joined-wing flight demonstrator aircraft. Configurations with a lower vertical tail and fairings over the main landing gear were compared with a recommendation on the combination had the best drag and dynamic stability characteristics. The dynamic stability analysis was broken into four key parts: a twist test experimentally measured mass moments of inertia, a panel method was used to find non-dimensional stability derivatives, lateral and longitudinal state space models estimated dynamic stability characteristics and handling quality levels were evaluated using a Cooper-Harper based rating system. VA-1 was found to have good longitudinal and lateral flight qualities for cruise flight. The lower vertical tail could be removed to reduce weight and drag without degrading dynamic stability. Spanwise lift coefficients for different wing sections in trimmed steady state turns at 50 and 55 degrees of bank were estimated to see which sections of the wing stalled first. The analysis revealed VA-1 can turn using bank angles less than 50 degrees without stall and that stall first occurred at the aileron, immediately outboard of the wing joint.

Acknowledgments

I would like to express my sincere appreciation to my faculty advisor, Dr. Robert Canfield, for his guidance and support throughout the course of this thesis effort. His insight and experience was certainly appreciated. I would, also, like to thank my sponsor, Dr. Maxwell Blair, and his many coworkers from the Air Force Research Laboratory Air Vehicles Directorate for the tremendous support they provided to me in this endeavor.

William A. McClelland

This Note is not to be included with the Acknowledgments – it is for information only: ***It is prohibited to include any personal information in the following categories about U.S. citizens, DOD Employees and military personnel: social security account numbers; home addresses; dates of birth; telephone numbers other than duty officers which are appropriately made available to the general public; names, locations and any other identifying information about family members of DOD employees and military personnel.***

Table of Contents

Page

Page

List of Figures

Figure Page

List of Tables

List of Symbols

Symbol	Definition	Units
a	speed of sound	(ft/s)
AR	Aspect Ratio	(-)
c	Chord	(ft or in)
C_{l_p}	variation in roll moment coefficient with respect to non-dimensional pitch rate	(1/rad)
C_{l_r}	variation in roll moment coefficient with respect to non-dimensional yaw rate	(1/rad)
C_{l_β}	variation in roll moment coefficient with respect to sideslip	(1/rad)
$C_{l_{\delta a}}$	variation in roll moment coefficient with respect to aileron deflection	(1/rad)
$C_{l_{\delta r}}$	variation in roll moment coefficient with rudder deflection	(1/rad)
C_{L_q}	variation in lift coefficient with non-dimensional pitch rate	(1/rad)
C_{L_α}	variation in lift coefficient with angle of attack	(1/rad)
$C_{L_{\dot{\alpha}}}$	alpha dot derivative	(1/rad)
$C_{L_{\delta e}}$	variation in lift coefficient with elevator deflection	(1/rad)
C_{m_q}	variation in pitch moment coefficient with non-dimensional pitch rate	(1/rad)
C_{m_α}	variation in pitch moment coefficient with angle of attack	(1/rad)
$C_{m_{\dot{\alpha}}}$	variation in pitch moment coefficient with time rate change in angle of attack	(1/rad)
$C_{m_{\delta e}}$	Variation in pitch moment coefficient with elevator deflection angle	(1/rad)

C_{n_p}	variation in yaw moment coefficient with non-dimensional roll rate	(1/rad)
C_{n_r}	variation in yaw moment coefficient with non-dimensional yaw rate	(1/rad)
C_{n_β}	variation in yaw moment coefficient with sideslip angle	(1/rad)
$C_{n_{\delta a}}$	variation in yaw moment coefficient with aileron deflection angle	(1/rad)
$C_{n_{\delta r}}$	variation in yaw moment coefficient with rudder deflection angle	(1/rad)
C_{y_β}	variation in side force coefficient with sideslip angle	(1/rad)
$C_{y_{\delta r}}$	variation in side force coefficient with rudder deflection angle	(1/rad)
I	mass moment of inertia	(slug-ft^2)
I_{xx}	mass moment of inertia about x axis	(slug-ft^2)
I_{xz}	cross product of inertia	(slug-ft^2)
I_{yy}	mass moment of inertia about y axis	(slug-ft^2)
I_{zz}	mass moment of inertia about z axis	(slug-ft^2)
l	hanging length	(ft)
M	Mach Number	(-)
P	period	(s)
p	pitch rate	(deg/s)
q	roll rate	(deg/s)
r	yaw rate	(deg/s)
r	radius of rotation	(ft)
Re	Reynolds Number	(-)
S	total wing area	(ft^2)
S_F	area of front wing	(ft^2)
SM	static margin	(-)
S_R	area of aft wing	(ft^2)
W	aircraft weight	(lb_f)

α	angle of attack	(deg)
β	sideslip angle	(deg)
ε	downwash angle	(deg)
$d\varepsilon/d\alpha$	Change in downwash angle with respect to angle of attack	(-)
Γ_F	front wing dihedral	(deg)
Γ_R	rear wing dihedral	(deg)
Λ_F	front wing sweep	(deg)
Λ_R	rear wing sweep	(deg)

INERTIA MEASUREMENT AND DYNAMIC STABILITY ANALYSIS OF A RADIO-CONTROLLED JOINED-WING AIRCRAFT

I. Introduction

A joined-wing aircraft has a swept forward tail that attaches to the forward wing forming a diamond-like shape. The inventor of the joined-wing concept, Julian Wolkovitch, initially introduced this design as more structurally and aerodynamically efficient than conventional wing-tail designs [4]. Potential uses for such a configuration include commercial transport or intelligence surveillance and reconnaissance (ISR). In the post 9/11 era, unmanned aerial vehicles (UAV) have increasingly been used to provide intelligence used for U.S. Military operations in Afghanistan and Iraq. One limitation to UAV data collection was a lack of ability to penetrate dense foliage. A conformal radar antenna array embedded in such a wing-tail combination could afford 360 degree radar coverage with improved ability to see through thick forest canopies. This configuration is commonly referred to as a Sensorcraft and is a current area of research at the Air Force Research Laboratory (AFRL).

Most joined-wing designs incorporated high aspect ratio, (*AR*), wings which were prone to aeroelastic effects. Complex interactions between aerodynamic forces, wing bending and twisting, structural weight, and direct operating cost savings spurred a series of researchers to investigate these phenomena and perform several trade studies. For the sensorcraft in particular, wing bending and twisting would deform the antenna array and

warp the radar picture as a result. In general, joined-wing research found: lower drag in certain cruise conditions, good stability characteristics at low angles of attack, and potential to control wing twist with active wing technology.

Figure 1. VA-1 Remote-Controlled Joined-Wing Aircraft [29].

In 2004 and 2005 AFRL Air Vehicles Directorate designed, built, and flew a scaled radio-controlled joined-wing aircraft, called VA-1, to explore structural integrity, aerodynamic stability and performance of a joined-wing configuration. Flight tests were suspended after the model landed hard after an apparent stall during a turn maneuver.

The flight test video revealed the following sequence of events leading to the hard landing. During a shallow right turn the starboard wing dipped slightly. The right hand bank became steeper as VA-1 lost altitude. VA-1 began to simultaneously pitch up and level its wings. Almost as soon as the wings became level, a loss of airspeed was noted and the aircraft descended quickly in an apparent stall while maintaining a small pitch angle. The plane was just beginning to pitch over when the ground came rushing up and

VA-1 rotated to land on the main landing gear. Figure 1 shows VA-1 immediately prior to the hard landing.

The intent of this research is to complete a dynamic stability analysis and investigate the potential stall that led to the hard landing. A preliminary stability analysis was conducted prior to flight test, however, was not completed due to lack of inertia data. The contribution of the lower vertical tail (LVT) to stability was also not analyzed before the test. The apparent trigger event that led to the hard landing was the starboard wing dip in the shallow turn. The exact cause of the wing dip was unknown but stall was suspected. This analysis would give the flight test team information to assess the risk of any potential future testing. In the case where flight testing does not continue this research will still provide useful information regarding dynamic stability and stall development for joined-wing aircraft.

VA-1 seemed underpowered despite having the most powerful electric motor practicable. Methods to reduce drag were also considered along with the analysis to improve performance in the event of future flight tests. Specifically, drag of the LVT and landing gear fairings will be considered along with their contributions to handling qualities of VA-1. The configuration that provided the best combination of drag and stability will then be recommended.

Predicting the dynamic stability for VA-1 required a great deal of information obtained from different methods. Figure 2 outlines the process both for dynamic stability and the stall analysis. Examining VA-1 geometry played an important role in ensuring the HASC model represented the aircraft well. Then aerodynamic coefficients were determined using a vortex-lattice method computer code called HASC-95 [20]. HASC output was used to calculate non-dimensional stability derivatives. A trim calculation used these derivatives to predict the cruise angle of attack and trim conditions for steady state level turns of various bank angles. Drag was modeled by computing parasite drag on the wing, fuselage and vertical surfaces with empirical equations. Induced drag was found from HASC output with the cruise angle of attack. In order to evaluate dynamic stability, the mass moments of inertia of VA-1 were also required and measured experimentally. Inertia data, combined with stability derivates and the drag model, were input into a decoupled lateral and longitudinal 3-DOF state space model to estimate dynamic stability characteristics in straight and level flight. VA-1 was approximated as a rigid body and propeller effects were neglected. Dynamic stability characteristics of different combinations of aerodynamic surfaces were considered and recommendations made regarding which surfaces should be used or discarded for any potential future flight of VA-1.

Once the HASC model was set up as desired the stall analysis became relatively straightforward. Spanwise lift coefficients during a trimmed steady state turn were examined to see which wing sections potentially stalled first and to find the bank angle

where stall began. For this process, trim conditions for the angle of attack, sideslip angle, all control deflections and angular rates were calculated for steady state level turns at different bank angles. The bank angles were increased until one or more wing sections stalled. This yielded the approximate bank angle for stall and located the wing section where stall began.

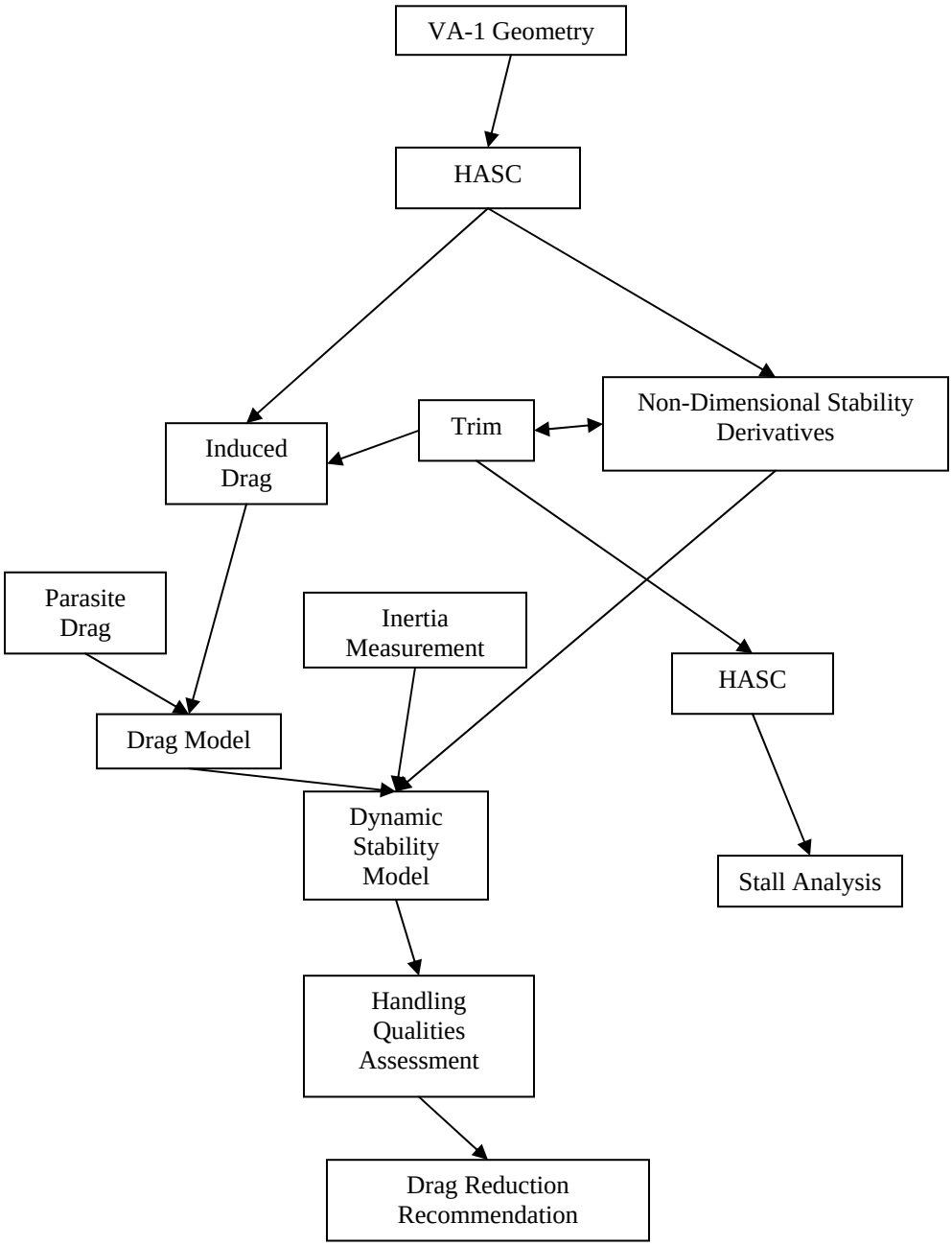

Figure 2. Research Process.

II. Literature Review

Chapter Overview

The purpose of this chapter is to discuss past research efforts regarding joined-wing aircraft. Most research efforts involved the interaction between structure, aerodynamics and operating cost. Research efforts are broken into three categories. Early research, AFIT research and AFRL research.

Early Research

Wolkovitch first introduced the joined-wing concept in 1976. He published some of his research findings later in 1986 and described the potential benefits of the joined-wing configuration [4]. He found that joined-wing aircraft could to be up to 25% lighter and have less induced drag than a conventional wing-tail design. The weight savings were contested by Samuels [1] and by Gallman [6]. Wolkovitch also claimed the configuration possessed good stability and control characteristics [4]. Smith *et al*, however, discovered a pitch up instability near stall angles of attack [5]. The optimal joint location was found to be from 60-100% of the span. For stability, Wolkovitch recommended the front wing stall slightly before the aft wing achieved C_{Lmax} [4].

Samuels reported a slightly lower structural weight savings than Wolkovitch regarding joined-wing design. She found a joined wing was 12-22% lighter than a reference, Boeing 727, conventional wing plus tail combination. The study was conducted by building a finite-element model of each respective wing and comparing the weights of them both [1].

Gallman, Kroo and Smith published research results of an aerodynamic and structural study of joined-wing aircraft. The most promising joint location appeared to be between 60-75% of the semi span. High aft wing compression forces were discovered and Gallman recommended examining aft wing buckling in closer detail. The authors concluded the joined-wing configuration had no real significant advantages over its conventional counterpart, but that the joined-wing concept was definitely worth further investigation [6].

Kroo, *et al* later conducted a structural study that accounted for the structural weight needed to prevent aft wing buckling [25]. In their study the aft wing was used for both pitch control and structural support for the forward wing. In comparison to an equivalent conventional design, they discovered the joined-wing needed a larger forward wing to improve takeoff field length performance and a larger tail to prevent buckling. The extra weight yielded a 3.2 % higher direct operating cost for the joined-wing. They concluded the joined-wing design was inferior to a comparable conventional wing.

Smith, Cliff and Kroo designed a joined-wing flight demonstrator aircraft called JW-1 and successfully tested a one sixth scale wind-tunnel model of their design. In the design stage they used a vortex-lattice method (VLM) program called LinAir to obtain aerodynamic lift and drag coefficients and found reasonable agreement with wind-tunnel data. By contrast, this research used the VLM approach with a different program called HASC and did not verify the computations with wind tunnel tests. Wind tunnel

tests revealed that JW-1, with vortilons added had satisfactory flying qualities for a flight demonstrator aircraft [5].

The JW-1 wing had a linear twist distribution to minimize induced drag with an elliptical lift distribution. A secondary objective of the twist was to achieve takeoff and landing without the fuselage hitting the ground. However, the swept and tapered high aspect ratio wing led to a minor unstable pitch up during stall. Wolkovitch, by contrast, simply stated that joined wings in general would have good stability and control characteristics and did not address this issue [4]. Wing twist was adjusted, at the cost of increased induced drag during cruise, to maintain good handling qualities and improve stall behavior [5]. VA-1 was similar to JW-1 in many aspects. A detailed comparison is made in the detailed geometrical description of VA-1. One key difference was that VA-1 had zero aerodynamic and geometric twist. As a result VA-1 is expected to have a less stable pitch up near stall angles of attack than JW-1.

JW-1 design modifications failed to completely eliminate the unstable stall problem and it re-emerged during wind-tunnel tests. Vortilons were installed on the front wing and produced a “profound improvement” in the post-stall pitching moment. Smith, *et al* also found the positive dihedral effect from the wing was reduced as the wing stalled and the lateral stability above stall was influenced by the negative dihedral contribution from the tail. They concluded the impact of this loss on lateral stability on the post-stall handling qualities should be investigated [5].

In the end Smith, Cliff and Kroo sacrificed cruise performance to get better stall characteristics as good handling was considered more important. On its final flight the VA-1 experienced an unrecoverable stall during a turn, resulting in a hard landing that suspended flight testing indefinitely. This study did not address post stall pitch up characteristics as HASC does not model viscous effects. However, a preliminary analysis of stall during turns was conducted.

Nangia *et al* examined configurations and conducted design studies of high aspect ratio sensorcraft vehicle. He evaluated uncambered wing sections and then wings with designed camber and twist using an inverse design method. He found aerodynamic interference effects between the wing and tail. For an uncambered configuration the leading edge suction was higher on the outboard tip of the front wing, whereas it was higher at the root of the aft wing. In addition, the wing tip experienced a higher loading than expected for an elliptical lift distribution. This effect was reduced when twist and camber were modified to make the spanwise lift more elliptical. Finally, an inverse wing design method using 3-D membrane analogy for joined-wings was discussed. Nangia demonstrated this design method's ability to quickly design wing twist and camber distribution [7].

Nangia *et al* examined six different Joined-Wing planforms and their effects on aircraft performance both at cruise, takeoff and landing. The configurations included forward and aft swept outer wing versions of a constant chord planforms, $AR = 17.46$, with leading edge extensions at fore and aft wing roots, and the "lambda-joined-wing"

concept. They assumed laminar flow during cruise and examined thick laminar flow airfoil wings both with and without camber. They found that the constant chord planforms, with optimized twist and camber to achieve laminar flow during cruise, had the lowest drag. This planform geometry was similar to the VA-1 planform, except the AFRL version has no variance in camber, zero twist and had a lower aspect ratio, AR = 14. Both AR calculations utilized combined front and aft wing areas [15].

Reich *et al* studied the idea of an Active Aeroelastic Wing control method to control wing and therefore antenna deformation. Their study found that six control surfaces could feasibly minimize antenna deformations while simultaneously trimming the aircraft. Furthermore they performed three more variations of progressively subdividing the control surfaces into smaller sections, gradually approaching a morphing type of wing [7].

AFIT Research

Smallwood examined, first, how effective an embedded antenna array in a rigid joined-wing type aircraft might be and, second, compared those results to an elastic array with wing twisting and bending. He found that radiation patterns of an array that conformed to the surface of the front end aft wing section of the joined-wing underwent significant distortion due to typical wing deflections. Smallwood recommended active control of wing deformations as a method to improve beam steering but stated that structural changes may also be needed [12].

In her work, Sitz looked at the effectiveness of control surfaces used for roll and lift on a joined-wing aircraft. Her goal was to determine the best location for adequate control that averted control reversal. She found that, if used, conventional control surfaces were best placed on the outboard wing and concluded that conventional control surfaces on the inboard fore and aft wing sections may be unusable due to radar requirements. VA-1 did not strictly follow these criteria as it utilized a trailing edge flap device for elevator on its rear inboard wings. An alternative control method, twisting the rear wing, fell outside the scope of her study and she recommended further analysis in that area [13].

Rasmussen sought a weight optimized configuration of a joined-wing aircraft by varying the following six wing design parameters: front wing sweep, aft wing sweep, outboard wing sweep, joint location, vertical offset and thickness to chord ratio. He determined the optimal weight design had either high vertical offset and low thickness to chord ratio, or low vertical offset and high thickness to chord ratio. He found the joint should ideally be located between 50% and 75% of the span. He also recommended avoiding high wing sweep angles for both the fore and aft wings [14].

Craft researched three different conceptual design methods for predicting drag of joined-wing type aircraft. His most accurate prediction method was broken into three parts. Wing drag was computed in the Aerospace Vehicle Technology Integration Environment, AVTIE. AVTIE, created by Dr. Maxwell Blair, used Pan Air to predict wing induced drag and XFOIL to determine wing parasite drag [98]. Since AVTIE only

accounted for the wing, Roskam's drag buildup approach was then used to find the drag of the fuselage and vertical tail. Total aircraft drag was the combination of wing, fuselage and vertical tail drag. Craft recommended a CFD analysis to validate his drag predictions [16].

This research used a similar approach to modeling the drag of the different configurations. Craft found that Roskam's method for finding induced drag on the wing was not as accurate as a panel-method computer code [16]. For this research, HASC was used to determine the induced drag of the front and rear wings, while Roskam's drag buildup approach was used to determine parasite drag caused by the wings, fuselage, vertical tails and landing gear.

AFRL Research

Due to initial concern regarding yaw stability, Bowman conducted a preliminary stability analysis on the AFRL Radio-Controlled Joined Wing aircraft [11]. He utilized HASC [20], a vortex-lattice panel method computer code to predict the forces and moments on the aircraft in flight. The aircraft center of mass was varied longitudinally from 47 to 51 inches aft of the nose and several different combinations of aerodynamic surfaces were examined to include: reference geometry, reference geometry and fuselage, reference geometry and ventral fins, reference geometry and winglets and finally reference geometry and main gear strutfins.

He concluded yaw stability, even with stability augmentation and strut fins, was likely too low for good flying qualities. In addition, at high angles of attack the yawing

moments became small. Since typical values of yaw moment due to sideslip range from 0.05 to 0.1 and higher values should be expected for radio-controlled aircraft, Bowman argued, artificial yaw damping should be used. Furthermore, the modifications used to fix the yaw damping in his analysis caused the spiral mode to become neutral or divergent and the modified vehicle would likely be prone to graveyard spirals [11]. This research will address VA-1 lateral stability in more detail.

Bowman predicted a longitudinally stable aircraft with Static Margin of 4% at the reference center of mass position. He stated that RC models typically need a static margin closer to 10% for the pilot to feel comfortable. He predicted a pitching moment coefficient below zero as long as the center of mass remained forward of a point approximately 50 inches aft of the nose. The fuselage was found to be destabilizing and he recommended the addition of winglets or strut fins, unless the center of mass was shifted forward [17].

Throughout his analysis it became clear that VA-1 stability was very sensitive to center of gravity location. Placing the center of mass too far forward made takeoff rotation difficult and too far aft made the plane unstable. For this reason, and to gather good inertia data, accurately measuring the center of mass became an important part of this research effort.

Bowman recommended simultaneous outboard aileron and rear wing elevator deflection for pitch control [11]. The inboard ailerons on the front wing section were used bilaterally for roll. This control scheme was used for the flight test and

subsequently used when determining the stability derivatives with respect to aileron flap deflection.

Inertia Measurement Methods

Miller researched a method for experimentally measuring aircraft inertia to within 1% of the actual value [1]. Hardware was built to limit oscillation to two dimensions and improved the accuracy of the measurements. Due to time and budget limitations the exact same hardware was not recreated for the VA-1.

In the report Miller utilized two methods to measure inertia: a pendulum method and a bifilar torsion pendulum. In both tests the aircraft was suspended by two cables. The pendulum method swung the aircraft side to side like a pendulum on a clock. The bifilar torsion pendulum measurement involved twisting the vehicle in a circular motion so that the center of mass remained equidistant between the suspension cables at all times. By measuring the axis of rotation relative to the attachment points and timing a predetermined number of oscillations the mass moment of inertia was calculated [1]. The VA-1 inertia measurement was based on this approach with some modifications discussed later.

III. VA-1 Geometry

Analysis of VA-1 geometry was important for ensuring the HASC model matched the actual dimensions as closely as possible. The VA-1 was a seven percent scaled model of a larger design [30]. It had a takeoff weight of 31.5 lbs, 168 in. wingspan and an 80 in. long fuselage. The 2.95 horsepower electric power plant was a MaxCim MegaMax 3.7 Brushless Motor installed in a pusher configuration [29]. An inlet was placed just below the nose to provide cooling air to the electric engine. The cooling air was let out the tail end of the fuselage. A 28 in. propeller with an 18 degree pitch at the root was used during the flight test.

In the design stage the VA-1 initial takeoff weight was 26 lbs. The takeoff weight, however, increased slightly due to minor design modifications. After Bowman's stability analysis revealed a weakness in yaw stability, a lower vertical tail was added to simultaneously improve lateral stability and protect the propeller during takeoff rotation. Flight test video confirmed that the lower vertical tail would hit the ground on takeoff rotation and protected the propeller as intended. A Global Positioning System (GPS) recording device was added inside the fuselage. Finally, the number of batteries used was increased to extend the engine life during the test. The repairs made to reconnect the fuselage and lower vertical tail after the hard landing may have also slightly increased the aircraft weight. After the repairs were made and all of the interior components were in place, VA-1's weight increased to 31.5 lbs, which should represent the weight of the aircraft during flight test.

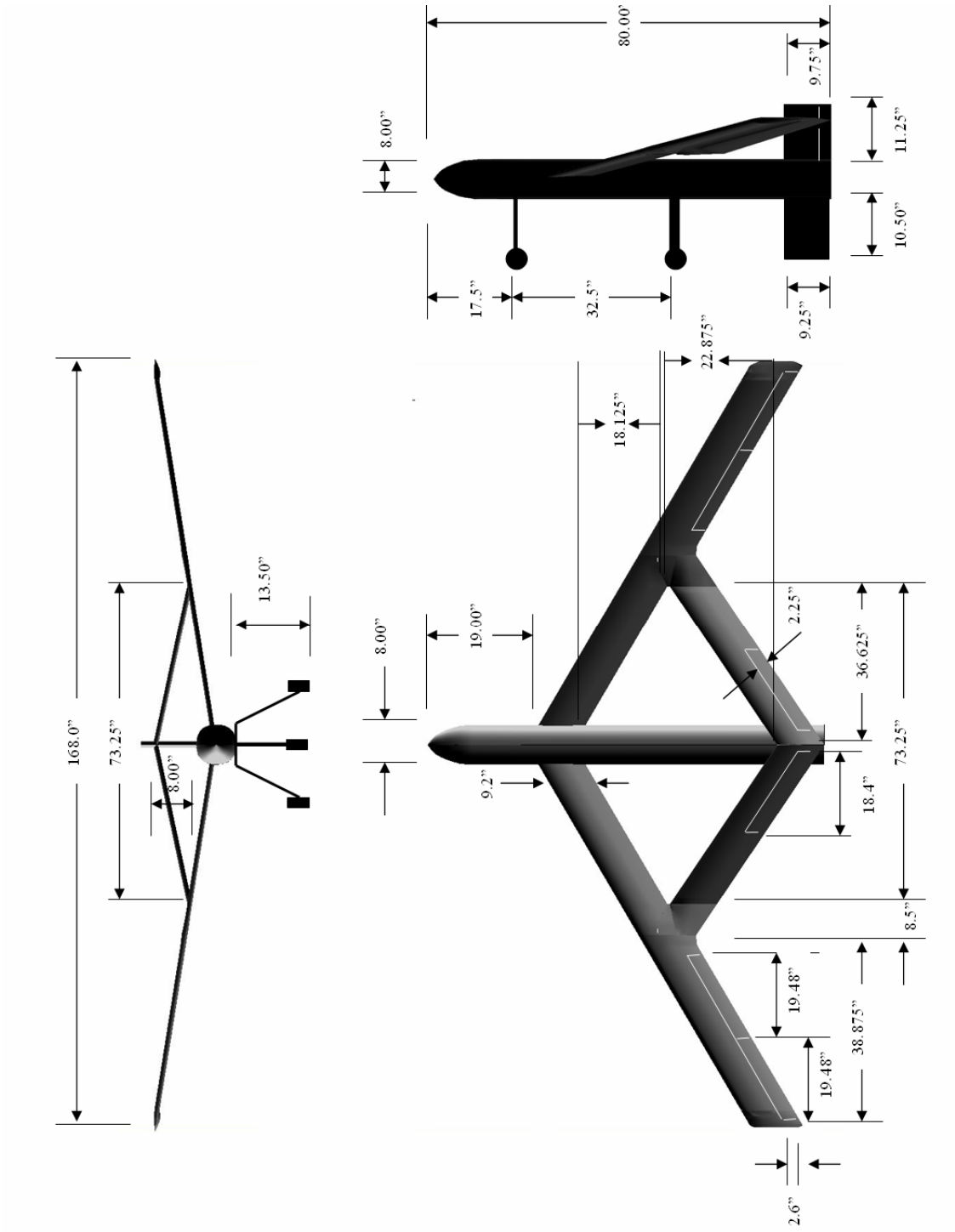

Figure 3. VA-1 Geometry.

The front and aft wings were created using a XF 60-100 airfoil shape with a constant streamwise chord of 9.24 in. The FX 60-100 airfoil was initially designed as a low-speed laminar flow airfoil. FX airfoils were named after Franz Xaver Wortmann, who designed the airfoils specifically for gliders. The nomenclature did not follow rigid guidelines, so not all designations had the same meaning. Usually the first two numbers designated the year of the design and the last three yield thickness in 1/1000's of chord [19]. The wings had a taper ratio of one and zero spanwise twist. Each wing section had the same camber along the span except at the joint, where the original camber was simply scaled to fit the new chord length and blended as smoothly as possible with the adjoining wing sections.

One area for potential confusion was the mean aerodynamic chord. The wing joint allowed a number of possible ways to compute the mean chord because it was part of both the front and rear wings. For this research, the mean aerodynamic chord was calculated from the front wing as though the rear wing did not connect at the joint. Since the root chord and tip chord were the same, the taper ratio was one. Hence the mean geometric chord was the same as the root chord, 9.24 in., and will be denoted as c in this study.

The front wing planform had 30 degrees aft sweep and the rear wing had 30 degrees forward sweep. Front and aft wing dihedral were 7.5 and -15 degrees respectively. The front wing leading edge started 19 in. from the nose and the rear wing leading edge started at 71.75 in. Vertically, the front wing root was positioned 1.6 in.

below the fuselage center line, while the aft wing root was 12 in. above the centerline. The front and rear wing sections joined at approximately 56% of the semispan. Note the VA-1 geometry was similar to the JW-1 geometry, tabulated for easy reference in Table 1. Stability derivatives will be compared later in the dynamic stability analysis. One crucial difference between the two designs was that the JW-1 wing was optimized in twist, airfoil and camber distribution to minimize induced drag and improve stability, while the VA-1 wing was not optimized in this way.

Table 1. Comparison of VA-1 with JW-1 [5].

Parameter	VA-1	JW-1
Λ_F	30º	30.5º
Λ_R	-30º	32º
Γ_F	7.5º	5º
Γ_R	-15º	-20º
AR	12.7	11.25
Joint Location (% semispan)	54%	60%
S_R/S_F	0.44	0.3
Re cruise	3.14×10^5	1.0×10^6
Static Margin, SM	0.4	0.35
Control Surface Chord (% of total chord)	28% (38% for rudder)	20%

There was potential for confusion regarding wing areas and aspect ratios. The term rear-wing will be used to denote the aft portion of the wing that is located where the horizontal tail would ordinarily be. The subscripts F and R were used to denote forward and rear wing sections respectively. Total wing area, $S = S_F + S_R$, was computed by combining the total planform surface area of both front and aft wings. The front wing

area, S_F, was computed as if only the front of the joint section existed and the front wing had a constant chord from the aircraft centerline to the outboard wing tip. The rear wing area, S_R, was simply the difference between the total area and the front wing. The aspect ratio, $AR = b^2/S$, was computed using total wing area. This wing area convention was used throughout this research effort.

From VA-1 geometry we can see that the spanwise lift distribution was not designed to be elliptic. This means that twisting the wing offers the possibility of both reduced induced drag and reducing a potential pitch-up instability near stall angles of attack. The zero twist possibly made the wing prone to tip stall, which in the case of VA-1, could cause loss of elevator effectiveness in stall. Smith *et al* discussed an unstable pitch-up problem when they built and collected wind tunnel data on their JW-1 design. They washed the forward wingtip in and the forward wing root out to reduce this effect. Eventually vortilons were added to bring the pitch up instability to acceptable levels [5]. Due to unique aerodynamic characteristics of joined-wing aircraft, careful wing aerodynamic design plays a critical role in flight worthiness of such aircraft. Redesigning the VA-1 wing with these aerodynamic effects in mind could yield both a drag reduction and improved stall characteristics.

V. Inertia Measurement

Chapter Overview

The purpose of this chapter is to discuss the method used to experimentally determine the inertia of VA-1. Inertia data along with non-dimensional stability derivatives are used to find dimensional stability derivatives used for the stability model. VA-1 inertia about the roll, pitch and yaw axes was measured using a twist test approach based on Miller's NACA TR 531. The fundamental premise of the test involved suspending an object from two points equidistant from the object's center of gravity. After the object was rotated by a small angle about its center of gravity and released, the period of oscillation was measured. The period, combined with other geometric dimensions, was then used to calculate inertia. Miller called this a bifilar torsion pendulum [1].

VA-1's large 14 ft. wingspan required a large open space to twist freely without obstruction or damage to the wings. The test was conducted in a large open room in AFRL's Bldg 65 at WPAFB as a result. A level I-beam, part of a crane, 23 feet off of the ground provided the ceiling attachment points. Nylon chords were tied to eye-bolts that were secured to the I-beam with I-beam clamps. Four clamps were spaced at specified intervals based on how the aircraft was suspended for each test so that the chord would be perfectly vertical when attached to VA-1. The cord attachment points were 29, 32 and 64.5 in. apart for the roll, yaw and pitch tests respectively. Cords were secured to

VA-1 in different locations and manners depending on which test was being performed. Figure 4 shows VA-1 suspended to measure inertia about the roll axis.

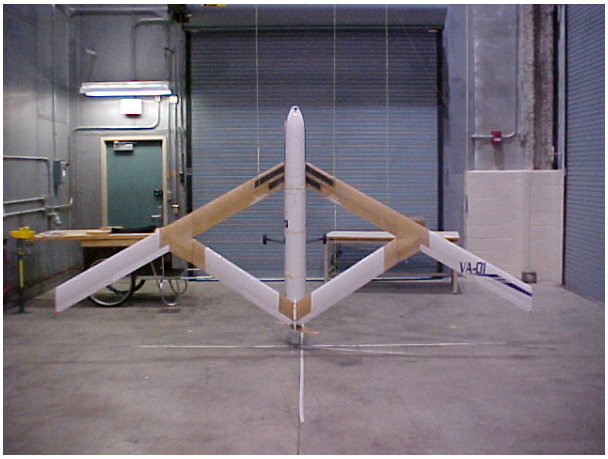

Figure 4. VA-1 Roll Inertia Twist Test Setup.

Validation Test

A cylindrical steel bar of uniform density was tested to verify the equation worked and the test setup could predict theoretical inertia within 10% uncertainty. The metal bar weighed 22.2 lbs, was 80.125 in. long and had a 1.125 in. diameter. Due to the length of the bar relative to its diameter, the theoretical inertia was calculated with the slender rod equation $I = (1/12)mL^2$ where m was mass in slugs and L was length in feet [16]. The theoretical inertia was found to be 2.56 slug-ft^2 with an uncertainty of 0.01 slug-ft^2. The experimental inertia, from the twist test, turned out to be 2.49 slug-ft^2 with an uncertainty of 0.04 slug-ft^2. The theoretical and measured values did not overlap exactly suggesting a phenomenon not modeled by the experiment equation. The difference may have been due to secondary oscillation. Also note the measured inertia

was similar in magnitude to VA-1 inertias. The experimental measurement showed a difference of 3% from the theoretical measurement and the test was found to be adequate for the purpose of this research.

The aircraft was measured with almost exactly the same procedures as the bar, except the orientations were different. Figure 5 illustrates how the bar was suspended from two cables with its center of gravity equidistant between the two attachment points. The bar's short axis, at the center of gravity, ran parallel to the vertical chords. The bar was then rotated about its c.g. to an initial position where its long axis was approximately ten degrees from the equilibrium position. The bar was carefully released and a stopwatch simultaneously started. The bar then twisted away from its initial release point and returned to its initial position. At the instant the bar changed directions after returning to the initial position, one cycle or oscillation was counted. The moment the object hit a predetermined number of oscillations, 50 cycles for the bar test, the stopwatch was stopped and the period was averaged over 50 cycles. This method, except for equipment setup, matched the NACA TR 351 almost exactly [1].

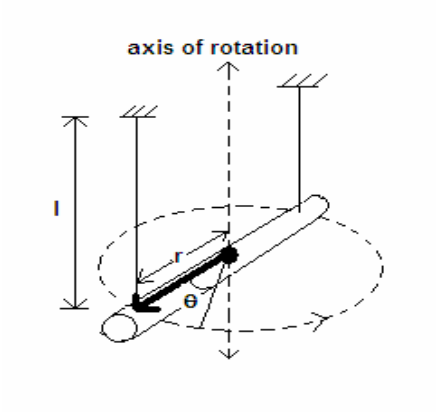

Figure 5. Twist Tests Setup for a long cylindrical bar.

The data was reduced in the following manner. The period was combined with weight, hanging length and radius of rotation to calculate the inertia about the measured axis with the following equation:

$$I = \frac{W}{l}\frac{r^2 P^2}{4\pi^2} \tag{1}$$

Where W is the weight in lb_f, r is the radius of rotation in feet, P is the period in seconds, l is the hanging length in feet, I is the mass moment of inertia in slug-ft^2. The hanging length was the length of the cord between the aircraft and the overhead attachment points.

This equation is not exactly the same as the inertia equation used for the bifilar torsion pendulum in Miller's report. His report used a value of 16 in place of the 4 [1]. Miller used the distance between the cables instead of the radius from the center of

gravity to one cable. Substituting a *(d/2)* for *r* would yield the exact same equation. The version in this research was preferred as it helped illustrate the location about which the body rotated. The interested reader is referred to Appendix A for a detailed derivation.

VA-1 Inertia Test

Centering the metal bar center of gravity between the chords was easy due to symmetry. VA-1 had an unusual geometry and heavy interior components that made predicting the center of gravity more difficult. In addition repairs to the front of the fuselage after the hard landing could have shifted the center of gravity. Figure 6 and Figure 7 show the fuselage repair work. The effect of the repairs on center of gravity, if any, was unknown. Aircraft c.g. was measured using two different methods to ensure accurate results.

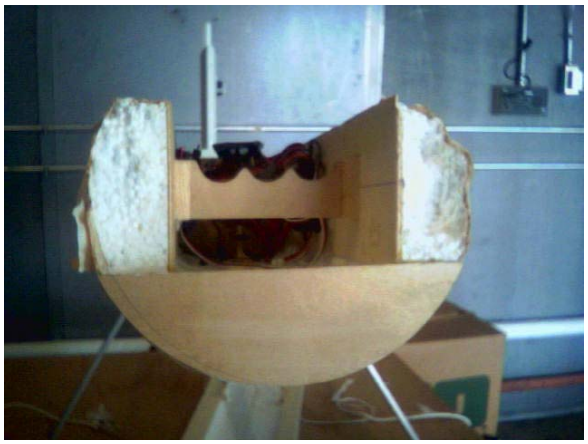

Figure 6. Fuselage Cross Section Prior to Completed Repairs.

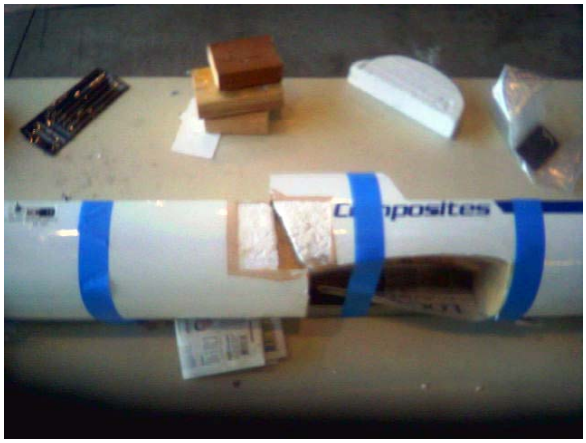

Figure 7. Fuselage Section Reconnected With Glue and Internal Braces.

Care was taken to match the internal configuration of VA-1 to that used for flight test so the measured inertia would match the flight test inertia. The aircraft was made with low density materials and redistribution of mass inside the fuselage could change both the inertia and the center of gravity. Batteries and the hand held GPS receiver were installed in the fuselage. The 28 in. propeller, damaged in the hard landing, was not used for the test. The closest available substitute, a 27 in. diameter propeller, was reattached to the shaft in its place. These components affected both weight and c.g., which in turn affected the inertia calculations.

The c.g. was first re-measured by hanging VA-1 from one chord tied around the fuselage and finding the point where the plane would balance on its own. Next, VA-1 was suspended by one chord at two separate attachment points in the same plane. A plumb line was hung from the attachment points and the angles of intersection with the

fuselage marked. The center of gravity was marked where the two lines crossed. This method had the added benefit of finding the $z_{c.g.}$ location. Both methods came within one inch of each other in the longitudinal direction and the $x_{c.g.}$ was marked 46.75 in. aft of the nose. This value was forward from the flight test value by approximately one inch.

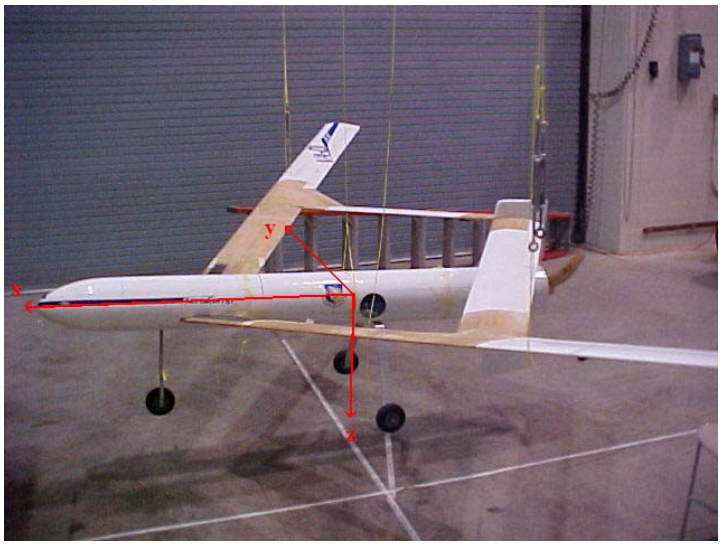

Figure 8. Center of Gravity Measurement with Body Axes Labeled.

VA-1 was suspended in three different orientations to measure three different inertias: I_{xx} , I_{yy}, and I_{zz} for roll, pitch and yaw respectively. Inertia was measured about the aircraft body axes, anchored at the aircraft center of gravity shown in Figure 8. The x-axis pointed out the nose, the y-axis pointed towards the starboard wing and the z-axis pointed down. The cross product of inertia, I_{xz}, was assumed to be negligible due to aircraft symmetry and was not measured. The other cross product of inertia, I_{xy}, was assumed to be close to zero. For each test, the attachment method and location varied to ensure the c.g. was placed equidistant between the two chords.

For the yaw inertia test, VA-1 was suspended by tying cords around the fuselage with wings level and fuselage parallel to the ground. Figure 9 shows the yaw inertia test setup. The chords attached to the crane were then connected to the fuselage chords while the plane sat on a table. When the table was removed the plane was suspended with the fuselage level to the ground.

Figure 9. VA-1 Yaw Inertia Twist Test Setup.

To capture roll inertia, cords were tied directly to the wings so that that the c. g. in both the y and z directions was centered between the attachment points. Figure 4 shows the roll test setup. Wing dihedral limited this distance and the radius of rotation was the smallest of the three configurations. The chords were taped down to the wings to minimize travel during the test. As the plane twisted in this configuration, the wings moved normal to the airflow. Aerodynamic damping was a concern but the effects were difficult to predict. Significant twisting seemed to end almost completely after five oscillations, which suggested significant damping existed in the system. The five oscillation limit was highly repeatable.

Meirovitch's treatment of damping and logarithmic decrement was used to estimate damping and its effect on the period[33]. The logarithmic decrement gave insight into the amount of damping encountered during the roll inertia test. The equation for logarithmic decrement was $\delta = (1/n)ln(x_1/x_{n+1})$, where δ is the logarithmic decrement, x_1 is the amplitude of the first peak and x_{n+1} is the amplitude of the fifth peak. The variable x can also be thought of as the magnitude of the displacement of the aircraft cord attachment point from the equilibrium position. The integer, n, is the cycle number of the last peak minus the cycle number of the first peak. Because the roll twist test appeared to stop after five cycles, a 99% decrease in amplitude over five cycles was assumed. The fifth cycle had magnitude $x_5 = 0.01x_1$ where the subscripts represent the cycle number. For this case $n = 4$ and $\delta = 1.1513$. Damping ratio, ζ, was then computed using the logarithmic decrement:

$$\zeta = \frac{\delta}{\sqrt{(2\pi)^2 + \delta^2}} \tag{2}$$

For roll test the estimated damping ratio was 0.18. The damped natural frequency, ω_d, is related to the undamped natural frequency, ω_n, by $\omega_d = \omega_n\sqrt{1-\zeta^2}$ and $\omega_d = 0.9836\omega_n$ [33].

Equation 1 assumed that damping was small and the damped period was virtually the same as the undamped period. When damping seems significant, the undamped period, P_n, can be found from the observed or damped period, P_d. In general, the period, P, is related to frequency, ω, by $P = 2\pi/\omega$. The damped period can be computed with $P_d = 2\pi/\omega_d$. By substitution $P_d = 2\pi/(0.9836\omega_n)$. Because $\omega_n = 2\pi/P_n$ we find $P_n = 0.9836$

P_d. For the roll inertia test the observed period is approximately 1.6% smaller than the undamped period. This means the inertia is smaller by a factor of 0.9836^2 and decreases the computed inertia by approximately 3.3%. Before accounting for damping, the roll inertia comes out to be 3.29 slug-ft^2. After correcting for damping the roll inertia is approximately 3.18 slug-ft^2[33]. The corrected value was used for the stability analysis.

To capture pitch inertia the plane was suspended sideways with the fuselage parallel to the ground. The center of gravity, in the z direction, was not directly on the fuselage centerline. Simply tying the chords around the fuselage would have allowed the aircraft to tilt or wobble during the test. Eye bolts were installed in the fuselage along the x-y plane at the $z_{c.g.}$ location. Figure 10 shows the pitch test setup.

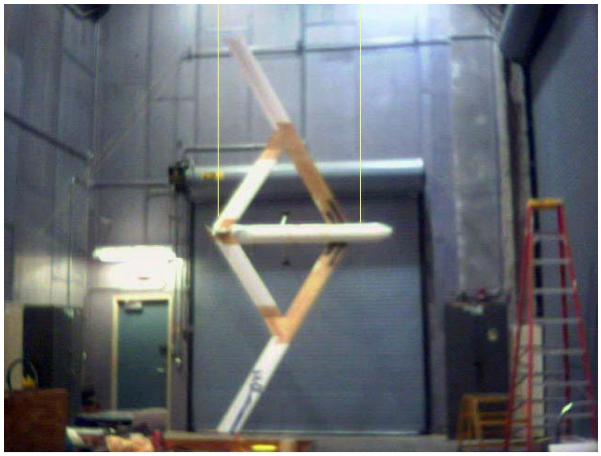

Figure 10. VA-1 Pitch Inertia Twist Test Setup.

To increase the accuracy of the results, a high number of oscillations were measured when possible. For example, during the yaw inertia measurement three sets of

fifty oscillations were timed. The total time divided by the total number of oscillations was then the average period, which was used for the inertial computation. This approach worked well for both the yaw and pitch inertias. The roll inertia, however, damped out almost completely in five oscillations so the period was adjusted for damping prior to inertia computation. The results are listed in Table 2. A description of the uncertainty analysis is given in Appendix A.

Table 2. VA-1 Twist Test Results.

Axis	Inertia (slug-ft^2)	Uncertainty (slug-ft^2)
Roll, I_{xx}	3.18	0.06
Pitch, I_{yy}	2.58	0.06
Yaw, I_{zz}	5.04	0.09

Several factors could have caused errors in the tests including secondary oscillations, damping and the cords. The aircraft c.g. did not remain perfectly centered during the test. Small side to side and front to back oscillations, called secondary oscillations, were noted. A possible cause may have been the non-zero cross products of inertia about the xy plane in addition to the unconstrained motion in more than two directions. The manner of release also seemed to impact the magnitude of secondary oscillation. At time test conductors accidentally imparted a velocity component during release. Tests were repeated according to the subjective criteria that secondary oscillations seemed too large. Some type of release mechanism may reduce this effect. These were probably the most significant sources of error.

Aerodynamic damping from the twisting motion may have impacted the roll. Simple equations for damping were used to correct the period of the roll test for the damping effect. For the pitch and yaw configurations damping was obviously negligible as the aircraft easily reached 50 oscillations for both tests.

Finally, the cords offered third source of error. A slight difference in hanging lengths on each side of the aircraft may affect the results as the axis about which the aircraft rotated should run precisely through the center of gravity. A level was used to ensure the hanging lengths were as even as possible. The nylon cords also stretched significantly, 6-8 in., from the weight of the plane. This may have been a source of damping, but the effects seemed insignificant. In addition the inertia of the chords was neglected in the analysis. Other errors may have come from errors in c.g. measurement. Despite these sources of error, the tests provided inertia data that was sufficient for the dynamic stability analysis.

VI. HASC Model and Stability Derivatives

Chapter Overview

This chapter discusses how the non-dimensional stability derivates used for the dynamic stability model were calculated. First, aerodynamic forces and moments for different combinations of angles of attack, sideslip angles and rotation rates were computed using HASC. Non-dimensional stability derivates were calculated from HASC output data using a excel spreadsheets that formed a derivative database. Many of the derivatives were slightly nonlinear with respect to angle of attack. The trim angle of attack for cruise, discussed in the next section, was iterated using the derivatives from this section and the associated non-dimensional stability derivates used for the dynamic stability model were linearly interpolated from the derivative database for the cruise angle of attack.

The HASC program utilized a Vortex Lattice Method (VLM) to compute aerodynamic coefficients for a given aircraft geometry. HASC-95, an updated version, was used for this analysis and will be referred to as HASC throughout this discussion. HASC uses three primary methods to solve for the aerodynamic coefficients: VORLAX, VORLIF and VTXCLD. VORLAX is a generalized vortex lattice program, VORLIF is a semi-empirical strake/wing vortex analysis code and VTXCLD is a two dimensional, unsteady, separated flow analogy program for analyzing smooth forebody shapes [20].

In this research VORLAX was used exclusively. Use of VLM on joined-wing configurations is not entirely without precedent. Smith *et al* found VLM could predict

aerodynamic coefficients for joined-wing type aircraft reasonably well [4]. This is probably because VLM method neglects both thickness and viscosity effects, which usually cancel each other out [23]. Due to the preliminary nature of the VA-1 as only a demonstrator vehicle, HASC was deemed an appropriate tool to estimate the aerodynamic stability derivatives.

HASC VA-1 Model

A HASC input file from Bowman's preliminary dynamic stability analysis was used as the baseline configuration. Bowman's inputs for vertical and horizontal fuselage segments, all wing surfaces and the upper vertical tail were used as the baseline configuration. Bowman's strutfin geometry was also used [11]. The strutfins could potentially be used as fairings covering the main landing gear struts and were modeled as small 4 x 10 in. flat plates with zero camber. The horizontal fuselage plane was used to capture fuselage effects for longitudinal derivatives. A lower vertical tail (LVT) and strutfins were evaluated as separate surfaces to determine their effect on the stability and drag. The LVT configuration represented the vehicle used for flight test.

The most significant addition to the HASC model was the lower vertical tail (LVT). Bowman did not analyze this surface in his report [11]. Other adjustments were also made to the model. The strutfins were moved forward to the main gear location used by the flight test team, as shown in Figure 3. Figure 11 shows both the LVT and strutfin locations on VA-1. All HASC inputs were closely verified from the actual vehicle. Wing geometry and camber remained unchanged. Propeller effects were neglected. The

rudder was resized so that it ran the full vertical distance of the upper vertical tail. The c.g. was moved from 48 in. to 46.75 in. from the nose for all cases to reflect measured c.g. used for the inertia tests. HASC computed the aerodynamic moments about this point.

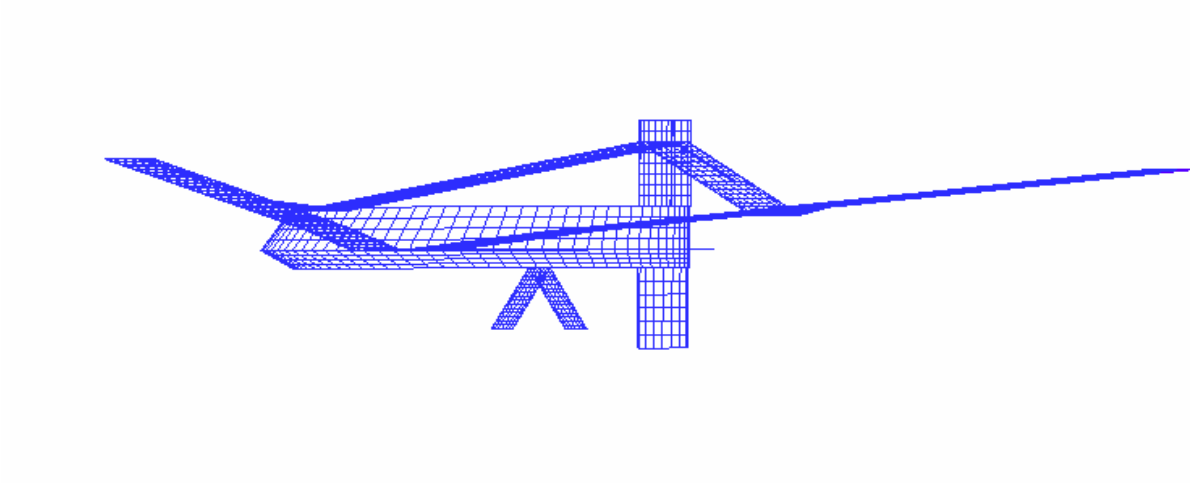

Figure 11. LVT and Strutfins on VA-1 HASC Model.

The preliminary flight conditions used for the previous analysis assumed a Reynolds Number, Re, of 300000 and a Mach Number of 0.065. Perhaps due to increased weight or higher than anticipated drag, the actual flight velocity was a bit lower than the 57 mph calculated in the initial cruise velocity analysis [31]. The Palm Pilot GPS data revealed, at the most consistent portion of the flight, an average speed of approximately 45 mph or 66 ft/s at full throttle was used. Note the GPS data sampling rate was not constant and varied between one and ten seconds. Using standard atmospheric data for a 1000 ft altitude and speed of 66 ft/s, Re was approximated as 314000 for a Mach Number 0.06.

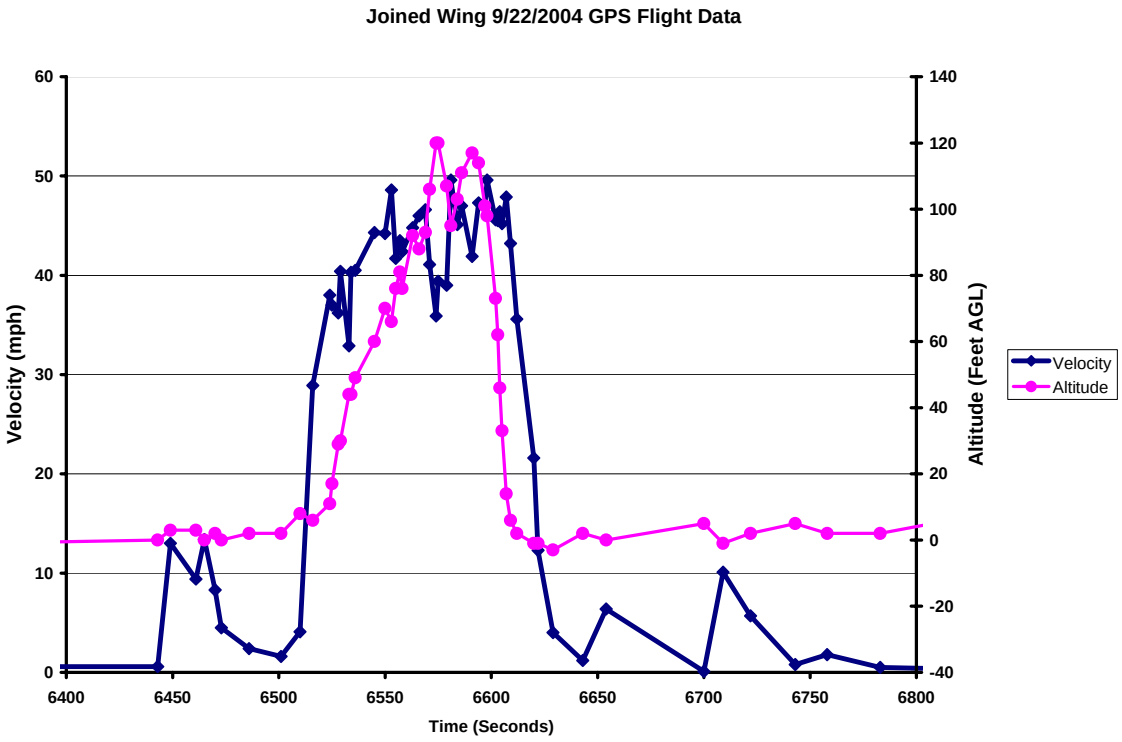

Figure 12. Palm Pilot GPS Data Reduced by AFRL Flight Test Team [36].

Each trailing edge device was assigned to one control function during the flight test. Figure 15 shows the elevators, ailerons and rudder control surfaces shaded green, red and blue respectively. Elevator control was assigned to the outboard control surfaces on the wingtips simultaneously with the trailing edge devices at the rear wing roots for a total of four elevator control surfaces. The rudder, on the vertical tail, ran the length of the vertical fin. Aileron control was bilateral movement of the inboard trailing edge devices on the front wings for a total of two surfaces. The ailerons were positioned inboard of the elevator surfaces at the wingtips. This was unusual because most aircraft utilize the outboard trailing edge flap for aileron control. Bowman found, in his HASC

analysis, the inboard aileron location was most effective for ailerons due to reduced lift at the wing tips [11]. This explains the unusual aileron placement.

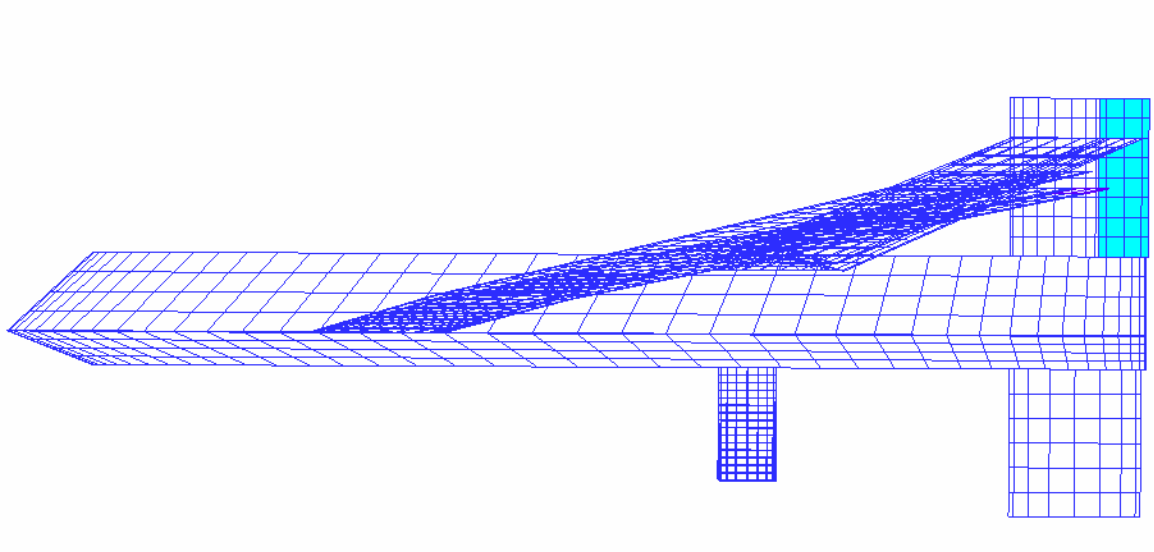

Figure 13. VA-1 HASC Model Sideview.

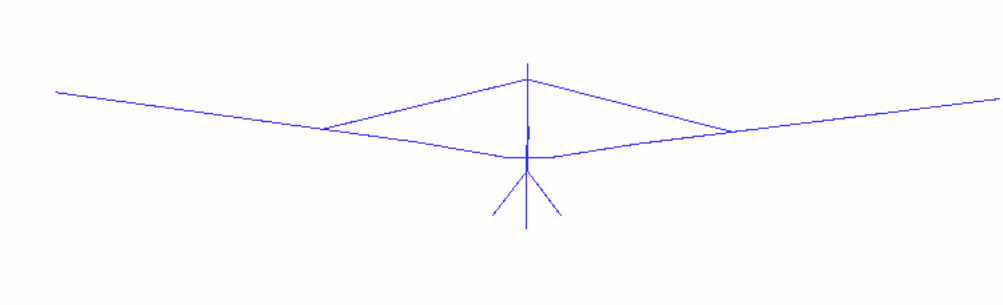

Figure 14. VA-1 HASC Model Frontview.

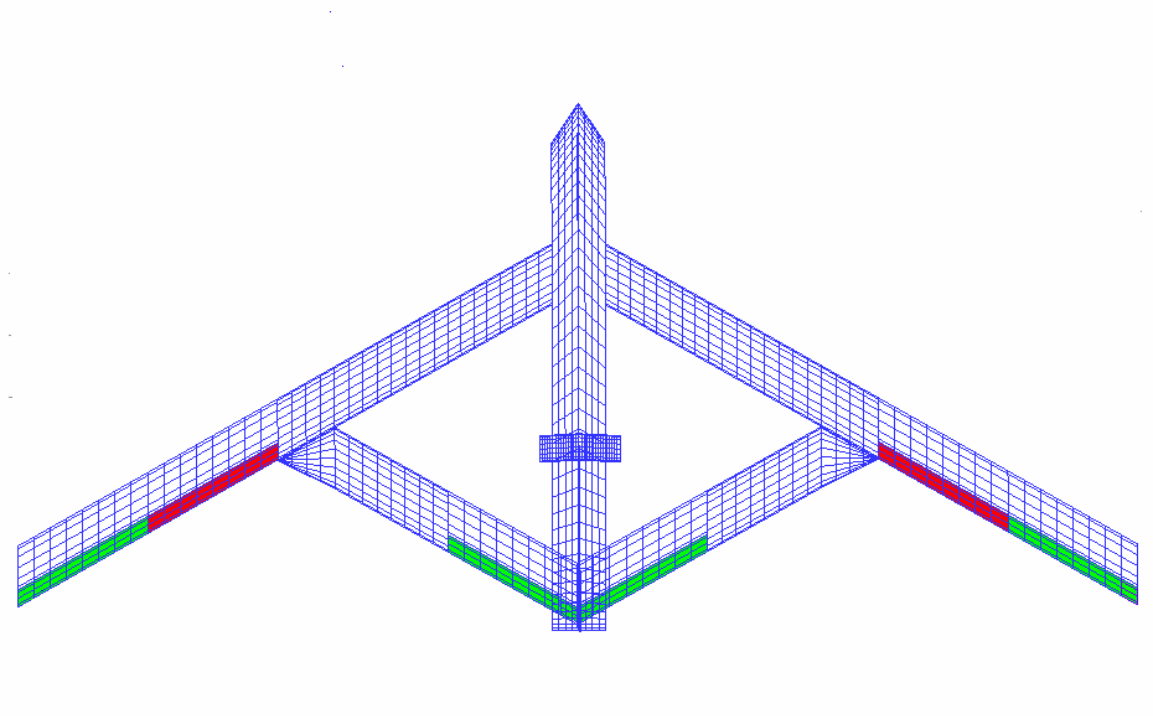

Figure 15. VA-1 HASC Model Top View.

Surfaces and Panels

HASC subdivides its surfaces and panels from largest to smallest with the following nomenclature: surfaces, panels, and subpanels [21]. VA-1 had eight surfaces: left forward wing (LFW), fuselage, right forward wing (RFW), left rear wing (LRW), strutfins, lower vertical tail (LVT), vertical tail, and right rear wing (RRW). Each surface was then divided into panels depending on its size. Control surfaces were modeled as separate panels. Chordwise divisions on the subpanels were distributed so a total of ten chordwise subpanels existed at any spanwise station on the wing. Figure 13, Figure 14 and Figure 15 show the panel distribution.

Panels were subdivided into subpanels by specifying the number of spanwise and chordwise divisions for each subpanel. In general, each wing subpanel had ten chordwise divisions. For sections of wing with trailing edge flaps, the ten chordwise divisions were distributed in a 60% - 40% fashion. The front wing and trailing edge subpanels had six and four chordwise divisions respectively. At the wing joints, spanwise divisions were carefully matched to line up with fore and aft panel sections. Table 3 lists the spanwise and chordwise panel distributions for the major surfaces.

An important part of the HASC model is airfoil camber. Bowman's camber inputs for the FX 60-100 Airfoil were used in this HASC model. For wing sections with trailing edge devices, the camber was superimposed across the combined for and aft sections. At the joint, camber was simply scaled to the new chord length. In Figure 9 shows the non-dimensional camber lines for three different airfoil sections in relation to the surface coordinates for the FX60-100 airfoil. The specific data points plotted represent actual camber ordinates input into HASC.

Table 3. VA-1 HASC Subpanel Distribution

Surface Name	**# of Surfaces**	**Spanwise Strips**	**Chordwise Strips**	**Subtotal**
Forward Wing	2	36	10	720
Fuselage	2	8	40	640
Rear Wing	2	20	10	400
Strutfin	2	15	8	240
LVT	1	6	8	48
Upper Vertical Tail	1	8	12	96
			TOTAL	**2144**

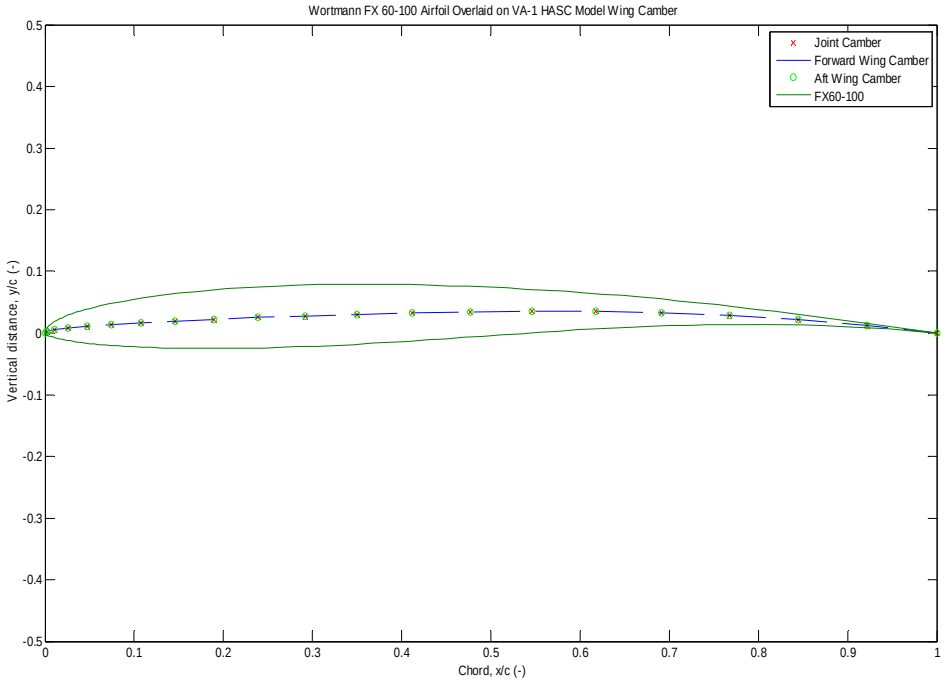

Figure 16. HASC camber lines compared to FX 60-100 Airfoil[38].

HASC outputs force and moment coefficients in the stability, wind and body axis systems. Stability axis coefficients were used to determine the non-dimensional stability derivatives. HASC used the total wing area, 2226 in^2, to non-dimensionalize its coefficients. The stability state space model used dimensional derivatives with respect to the body axis.

By comparison, Smith *et al* used VLM to analyze the JW-1 in LinAir. They input the complete aircraft geometry and had 20 spanwise by 5 chordwise panels for the front wing and 12 spanwise by 5 chordwise panels for the tail. Eight panels were used for the fuselage and engine nacelles for a total of 168 panels. The wind tunnel results for JW-1

matched the C_{m_α} and C_{L_α} predicted by LinAir fairly accurately between -4 and 3 degrees angle of attack [4].

HASC Test Matrix

A range of variables were altered to produce stability coefficients through a range of angles of attack, sideslip angles, roll rates, pitch rates, yaw rates, elevator and aileron deflection angles. Angle of attack, α, and sideslip angle, β, are in degrees. Positive angular rates mean right wing down for roll, nose up for pitch, and nose right for yaw. Surface deflections for elevator aileron and rudder are in degrees. Positive elevator deflection, δe, means trailing edge down. Positive aileron deflections, δa, were coordinated for a right roll. For example, an aileron deflection of five degrees was input as five degrees up on the right aileron and five degrees down on the left aileron. Positive rudder deflection, δr, means rudder trailing edge right and moves the nose right. This is opposite the normal rudder convention and more is discussed in the chapter on trim.

Entries with an arrow, →, denote a range of values incremented by the number after the comma, with the first and last value included. In the case where numbers were separated by commas, HASC did not automate the iterations and was run separately for each output.

Table 4 and Table 5 show the combinations of variables run in HASC to find lateral and longitudinal stability derivatives. For all longitudinal cases $\beta = p = r = \delta a = \delta r = 0$.

Table 4. HASC Test Matrix for Longitudinal Stability Derivatives.

Angle of Attack (deg)	Pitch Rate (deg/s)	Elevator Deflection (deg)
-5→10, 1	-5,0,5	0
-5→10, 1	0	-5,5

Table 5. HASC Test Matrix for Lateral Stability Derivatives.

Angle of Attack (deg)	Sideslip (deg)	Roll Rate (deg/s)	Yaw Rate (deg/s)	Aileron Deflection (deg)	Rudder Deflection (deg)
-4→8, 2	-5,0,5	0	0	0	0
-4→8, 2	0	-5,5	0	0	0
-4→8, 2	0	0	-5,5	0	0
-4→8, 2	0	0	0	-10,-5,5,10	0
-4→8, 2	0	0	0	0	-10,-5,5,10

HASC was used to find force and moment coefficients. The output files were put into an excel spreadsheet and stability derivates were computed by finding the slope between test points. For example, C_{L_α} was found by computing the rate of change in lift coefficient with respect to the change in angle of attack. Derivatives with respect to the angular rates *p*, *q* and *r* in radians/second were converted their corresponding non-dimensional roll, pitch and yaw rates: $pb/2u_1$, $qc/2u_1$ and $rb/2u_1$ respectively, where u_1 was the steady state velocity, *b* was the wingspan and *c* was the mean aerodynamic chord. The units for non-dimensional angular rates were found in radians and the units for their respective derivatives were reported in units of 1/rad. Because the derivatives varied slightly with angle of attack, the trim angle of attack was needed to determine the appropriate non-dimensional stability derivatives to use in the dynamic stability model.

Non-Dimensional Longitudinal Stability Derivatives

As expected, the LVT had virtually no effect on the longitudinal derivatives. Small, yet insignificant changes were noted due to the strutfins. Table 6 shows the differences in the non-dimensional derivative calculations between the baseline and strutfin configurations. JW-1 derivatives from wind tunnel data were also included for comparison. Units are 1/rad. Strutfins made the pitching moment derivatives slightly more negative and slightly increased C_{L_q}. $C_{m_{\dot{\alpha}}}$ was estimated as C_{L_q} ($d\varepsilon/d\alpha$) [18].

Table 6. Non-Dimensional Longitudinal Stability Derivatives For Different Configurations.

Derivative	Baseline	Strutfins	JW-1
C_{L_α}	4.842	4.888	4.64
C_{D_α}	0.426	0.428	0.267
C_{m_α}	-1.072	-1.093	-1.153
C_{L_q}	8.966	9.162	N/A
C_{m_q}	-25.593	-25.593	N/A
$C_{m_{\dot{\alpha}}}$	-15.708	-15.708	N/A
$C_{L_{\delta e}}$	0.7795	0.7795	0.2
$C_{m_{\delta e}}$	-1.5383	-1.5383	N/A

The change in downwash angle with respect to angle of attack, $d\varepsilon/d\alpha$, was found by comparing two HASC models: the first a rear wing and fuselage without a front wing attached, the second a complete front wing, fuselage and rear wing combination.

Downwash angle, ε, was found by observing how much the downwash from the front wing effectively reduced the angle of attack on the rear wing. This approach is similar to that used in wind tunnels [24].

First, the lift curve slope of the rear wing without the downwash effects of the front wing was found by removing the front wing from the HASC model. Aircraft angle of attack was fixed to zero degrees and rear wing incidence angle was set to zero and five degrees respectively. The slope of the change in rear wing lift coefficient, C_{L_R}, with respect to angle of attack, $\Delta C_{L_R} / \Delta\alpha$, was computed. At this point C_{L_R} without the front wing downwash is known for zero and five degrees angle of attack.

Next, with the front wing attached, C_{L_R} was computed at zero and five degrees angle of attack. With downwash effects of the front wing included, the new C_{L_R} values were slightly reduced from the case with the front wing removed. This reduction in C_{L_R} was due to downwash angle. The change in C_{L_R} was divided by the lift curve slope of the rear wing to find the change in angle of attack required to match the reduced lift coefficient. This change in angle of attack was the downwash angle. The change in downwash angle with respect to aircraft angle of attack was found by computing a downwash angle for two separate angles of attack:

$$\frac{d\varepsilon}{d\alpha} = \frac{\varepsilon_2 - \varepsilon_1}{\alpha_2 - \alpha_1}$$

Where ε_2 is the downwash when α = 5 deg and ε_1 is the downwash when α = 0 deg. For VA-1 $d\varepsilon/d\alpha$ turned out to be approximately 0.61.

Non-Dimensional Lateral Stability Derivatives

The different configurations had several noticeable effects on the lateral stability derivatives. Table 7 shows the results for all four configurations in units of 1/rad. Derivatives with respect to β seemed to vary the most. As expected, derivatives with respect to non-dimensional pitch rate did not change much. Some minor variations occurred in the derivatives with respect to non-dimensional yaw rate.

Addition of the LVT and strutfins made C_{y_β} more negative. This made sense as both surfaces increase the surface area facing the sideslip angle and more positive sideslip would generate more negative sideforce. A balance between C_{l_β} and C_{n_β} for good Dutch roll stability is required.

The dihedral derivative, C_{l_β}, became less negative as the LVT and strutfins were added. The dihedral derivative usually ranges from about -0.4 to 1.0 per radian [23] and VA-1 sits well in this range. The trend made sense because adding surface area below the fuselage centerline would cause a resistance to any rolling motion induced by sideslip. Think of the fuselage and one vertical tail on top. Positive sideslip would cause a negative roll moment, or a left roll. Now add a mirror image of the vertical fin pointing down. The roll moments caused by sideslip on both vertical surfaces would then tend to cancel each other out.

More negative dihedral derivative values usually mean the aircraft will be more stable in the Dutch roll mode. This means the LVT and strutfins tended to decrease Dutch roll stability with respect to this derivative. This was possibly due to the increased

weathercock stability caused by addition of vertical surfaces. In the case of a positive sideslip the aircraft would yaw more quickly to the right, due to the higher C_{n_β} term. As a result the left wing increases in speed and induces a right roll increasing the Dutch roll effect[24]. Table 7 shows C_{n_β} increased by 48% from adding the LVT. The strutfins increased yaw stiffness by approximately 8%. These effects seem reasonable as the yaw stiffness derivative is strongly influenced by the size of the vertical tail.

Table 7. Non-Dimensional Lateral Stability Derivatives for Different Configurations.

Lateral Derivatives	Baseline	LVT	Strutfins	LVT + Strutfins
C_{y_β}	-0.4688	-0.5658	-0.5651	-0.6602
C_{l_β}	-0.1437	-0.1374	-0.1378	-0.1309
C_{n_β}	0.0302	0.0449	0.0325	0.0472
C_{y_p}	-0.1066	-0.1111	-0.1066	-0.1111
C_{l_p}	-0.5147	-0.5147	-0.5147	-0.5147
C_{n_p}	-0.0019	-0.0019	-0.0019	-0.0019
C_{y_r}	0.2180	0.2829	0.2288	0.2937
C_{l_r}	0.1552	0.1552	0.1552	0.1552
C_{n_r}	-0.0344	-0.0452	-0.0344	-0.0452

The LVT made yaw damping , C_{n_r} , more negative by 31% and the strutfins had no effect. At first glance we expect the LVT be more stabilizing than the strutfins in the

Dutch roll mode. Yaw damping is usually the most important derivative for determining Dutch roll stability. It is important to note a balance between yaw damping and dihedral derivative, C_{l_β}, is required to achieve good Dutch roll characteristics[18]. The different configurations reveal the tradeoff: adding the LVT degrades the dihedral derivative in terms of stability while improving the yaw damping derivative. The dynamic stability analysis should reveal the end result of this tradeoff.

VII. Trim

Trimming the aircraft was critical for both the dynamic stability and turn analysis. Calculations for three types of steady state maneuvers were performed: steady state straight and level flight and a steady state level turn. Steady state means angular rates in addition to aircraft forces and moments remain constant throughout the maneuver. The trim angle off attack for straight and level flight was used to linearly interpolate the stability derivatives and induced drag used directly for the stability model. The steady state angle of attack, sideslip angle, control surface deflections and angular rates were required for the stall analysis. They were used to trim HASC model through a range of hypothetical bank angles. Then HASC was used to examine the spanwise lift distribution to see where stall might occur first.

The trim equations came from the aircraft equations of motion with respect to the stability axis. The equations used to trim for steady level flight were the same as the equations used for a steady level turn with a few exceptions. For straight and level flight the bank angle was set to zero, the load factor, n, was set equal to one and all of the angular rates and moments were zero. In general these equations assume the aircraft has adequate control power and the servos generate enough torque to maintain adequate control surface deflection [24].

Some assumptions were made to simplify the problem. First, the equations assumed flow remained attached over the wings. Since the purpose of the turn trim was

to see where stall developed first a potential limitation exists for this approach. Trim conditions for turns where a section of the wing exceeded the maximum lift coefficient, or stalled, would not be a realistic trim condition. Another assumption was that the stability x-axis stayed in the same plane throughout the turn. Stability derivatives were computed with respect to stability axes and no transformation was required for these equations. The roll rate, *p*, was assumed to be zero. For the steady state turn bank angles were assumed prior to solving the equations[24].

Roskam's steady state turning flight equations were used to find the trim conditions. Roskam included a term to account for the effect of the horizontal tail incidence angle, but those terms were neglected as the tail incidence angle for VA-1 was zero. These equations would need modification for a twisting rear wing or inclined horizontal tail. First finding the load factor *n*, as $n = 1/\cos\varphi$ where positive φ is the bank angle with the right wing down. The steady state pitch and roll rates, *q* and *r* respectively, can then be found as $q=g/u_1(n-1/n)$ and $r=(g/nu_1)\sqrt{n^2-1}$ where *g* is the gravitational constant and u_1 is the steady state velocity in ft/s[24:224-230].

Next we turn our attention to the trim angle of attack and elevator deflection angle for the steady state turn. The following equations were found by separating the longitudinal aerodynamic force and moment equations from the lateral equations. Assuming the aircraft had enough thrust to maintain the respective steady state condition, the remaining longitudinal equations could be solved with the following:

$$\begin{bmatrix} C_{L_\alpha} & C_{L_{\delta e}} \\ C_{m_\alpha} & C_{m_{\delta e}} \end{bmatrix} \begin{Bmatrix} \alpha \\ \delta e \end{Bmatrix} = \begin{Bmatrix} nC_{L_{trim}} - C_{L_0} - C_{L_{i_h}} i_h \\ -C_{m_0} - C_{m_q} \frac{cg}{2u_1^2}(n - \frac{1}{n}) \end{Bmatrix} \quad (3)$$

where $C_{L_{trim}}$ was the trim lift coefficient when lift equaled weight, C_{L_0} was the lift coefficient at zero angle of attack, C_{m_0} was the moment coefficient at zero angle of attack, c was mean geometric chord in feet, α was the angle of attack in radians and δe the elevator deflection angle, also in radians[24]. The term i_h was the incidence of the horizontal tail while $C_{L_{i_h}}$ was the change in lift coefficient with respect to change in horizontal tail incidence angle. The tail incidence for VA-1 was zero, but the tail incidence terms could perhaps be expanded for future use with a twisting rear wing. Note that positive elevator deflection means trailing edge down. Note once again, for steady level flight, when $n = 1$ the bottom right term on the right hand side become zero. At this point enough is known for trim in straight and level flight as the sideslip angle, aileron deflection and rudder deflection are all zero.

To complete the steady state turn trim we need to account for the sideslip angle, β, aileron deflection angle, δa, and rudder deflection angle, δr. From the lateral aerodynamic force and moment equations Roskam provides the following system of lateral equations[24:224-230]:

$$\begin{bmatrix} C_{y_\beta} & C_{y_{\delta a}} & C_{y_{\delta r}} \\ C_{l_\beta} & C_{l_{\delta a}} & C_{l_{\delta r}} \\ C_{n_\beta} & C_{n_{\delta a}} & C_{n_{\delta r}} \end{bmatrix} \begin{Bmatrix} \beta \\ \delta a \\ \delta r \end{Bmatrix} = \begin{Bmatrix} -C_{y_r} \dfrac{bg \sin\phi}{2u_1^2} \\ \dfrac{(I_{zz} - I_{yy}) g^2 \sin^3\phi}{QSbu_1^2 \cos\phi} - C_{l_r} \dfrac{bg \sin\phi}{2u_1^2} \\ -C_{n_r} \dfrac{bg \sin\phi}{2u_1^2} \end{Bmatrix} \qquad (4)$$

Recall Q was used for dynamic pressure in lb_f/ft^2 to avoid confusion with the pitch rate q.

The equations were solved with a MATLAB script file and simple matrix manipulation[27]. First, the equations were input into the form $Cx = b$, where C was the matrix of non-dimensional stability derivatives, x contained the unknown trim angles for the longitudinal or lateral equations. Then the term on the right hand side was premultiplied by the inverse of C, $x = C^{-1}b$, to find the steady state trim angles in radians. The angles were converted to degrees for ease of use later in the analysis.

Using the non-dimensional stability derivatives computed from HASC data for the LVT the trim conditions for bank angles of 0, 50 and 55 degrees were computed and presented in Table 8. For all cases the roll rate, p, was zero. For the zero bank angle the trim angle of attack was 2.36 degrees. This was the trim angle of attack for steady level flight and was used to interpolate the non-dimensional stability derivatives used for the model.

Since the stability derivatives had some mild non-linearities, the trim calculations for straight and level flight were iterated a couple of times. The first guess for trim angle of attack was made by simply computing the angle of attack that corresponded to the lift coefficient where lift equaled weight. The stability derivatives for $C_{L\alpha}$ and $C_{m\alpha}$ were

interpolated and fed into the trim equations above for straight and level flight. This of course did not account for elevator deflection and the next solution provided a more realistic angle of attack. By repeating the process until the trim angle of attack did not change by more than 0.01 degrees the aircraft was considered trimmed for straight and level flight. The rest of the non-dimensional stability derivatives were then found at the trim angle of attack and used for the dynamic stability model.

The steady state level turn trim conditions were not iterated in the same manner. The turn would require interpolating between more variables and quickly becomes much more complicated. Again, the purpose of the trim for turning flight was to examine spanwise lift distribution. Iterating would only cause minor changes in small control deflections and have little effect on the local lift coefficient. In addition, the trim angle of attack only slightly increased from straight and level flight. As a result the stability derivatives used to find straight and level flight were also used to find the trim conditions for each bank angle.

Table 8. Steady State Turn Trim Conditions Used for HASC Input.

Bank Angle	**0**	**50**	**55**	**(deg)**
Pitch rate, q	0.00	25.51	32.70	(deg/s)
Yaw rate, r	0.00	21.41	22.90	(deg/s)
Angle of Attack, α	2.36	5.82	6.96	(deg)
Sideslip Angle, β	0.00	-0.43	-0.66	(deg)
Elevator Deflection Angle, δe	-10.69	-15.57	-17.06	(deg)
Aileron Deflection Angle, δa	0.00	6.11	8.93	(deg)
Rudder Deflection Angle, δr	0.00	9.47	12.01	(deg)

VIII. Dynamic Stability

Dynamic stability of VA-1 was evaluated in the cruise flight condition for each configuration. VA-1 was assumed to be a rigid body and aeroelastic effects were neglected to simplify the model. Lateral and longitudinal flight dynamics were decoupled into two three-degree of freedom state space models of the form $\dot{x} = Ax + Bu$. The *A* and *B* matrices contained the dimensional stability derivatives and *x* was a state vector and *u* was a control vector. The corresponding eigenvalues of each system were used to determine the damping and natural frequencies of each flight mode. Longitudinal flight modes included the short period and phugoid modes. Lateral modes included roll, Dutch roll and spiral modes. The data for each mode was compared against longitudinal and lateral flying qualities to determine which combination of surfaces was best for inherent dynamic stability of the airframe.

Since stick-fixed stability was evaluated, the control matrix, *B*, was not needed. The longitudinal *A* matrix was estimated using dimensional derivatives and assumed Z_q and $Z_{\dot{w}}$ were negligible. The dimensional derivatives are with respect to the body fixed reference frame. To review the dimensional derivative nomenclature, *X*, *Y* and *Z* correspond to forces in the body axis *x*, *y* and *z* directions. Variables *L*, *M* and *N* represent the aerodynamic moments about the *x*, *y* and *z* axes. The subscripts *u*, *v* and *w* represent a derivative with respect to velocity in the *x*, *y* and *z* directions on the body axis. For these derivatives, subscripts *p*, *q* and *r* represent the dimensional derivatives with respect to the angular rates about the *x*, *y* and *z* body axes respectively. For example, the

derivative Z_q would be the change in aerodynamic force in the z-direction with respect to a change in pitch rate, q and is typically small for conventional fixed-wing aircraft. The subscript β is the derivative with respect to sideslip angle and the subscript *1* represents the initial unperturbed condition. The gravitational constant is denoted as g [18]. The longitudinal A matrix was:

$$A=\begin{bmatrix} X_u & X_w & 0 & -g \\ Z_u & Z_w & u_1 & 0 \\ M_u+M_{\dot{w}}Z_u & M_w+M_{\dot{w}}Z_w & M_q+M_{\dot{w}}u_1 & 0 \\ 0 & 0 & 1 & 0 \end{bmatrix} \tag{5}$$

and the corresponding states $x = [\Delta u\ \Delta w\ \Delta q\ \Delta\theta]^T$ [18:149]. The lateral modes were found with the following dimensional coefficient matrix:

$$A=\begin{bmatrix} \frac{Y_\beta}{u_1} & \frac{Y_p}{u_1} & -\left(1-\frac{Y_r}{u_1}\right) & \frac{g\cos\theta_0}{u_1} \\ L_\beta & L_p & L_r & 0 \\ N_\beta & N_p & N_r & 0 \\ 0 & 1 & 0 & 0 \end{bmatrix} \tag{6}$$

with the following states $x = [\Delta\beta\ \Delta p\ \Delta r\ \Delta\varphi]^T$ [18:195].

MATLAB was used to solve for the eigenvalues of the *A* matrices. Each A matrix had four associated eigenvalues. The longitudinal A matrix produced two short period and phugoid eigenvalues. The lateral A matrix produced a roll mode eigenvalue, usually the largest in magnitude, a complex conjugate pair of eigenvalues for Dutch roll and one smaller real eigenvalue for the spiral mode. The real and imaginary parts of the

eigenvalues were used to compute the different handling quality criteria for each mode. The natural frequency was $\omega_n = \sqrt{\mathrm{Re}^2 + \mathrm{Im}^2}$ and damping ratio was $\zeta = \cos\left(\tan^{-1}\left(\frac{\mathrm{Im}}{\mathrm{Re}}\right)\right)$. The eigenvalue real component was equal to $\zeta\omega_n$. Negative real eigenvalue components indicated a stable mode.

Dynamic Stability Criteria

General dynamic stability requirements for lateral and longitudinal modes can be referenced in MIL-STD-1797A Appendix A and appear in many aircraft stability and control texts[26]. MIL-STD-1797A was written primarily for manned aircraft so the criteria are inexact. For simplicity, this research focused on stick-fixed stability. Specific parameters used to determine flying quality levels depended on aircraft class and flight phase category.

Aircraft class takes into account aircraft size and weight. A small fighter aircraft has different stability requirements than a large heavy transport. The flight phase category takes into account pilot task requirements during different phases of flight. For example takeoff and cruise flight have different task requirements and impose different types of workloads for the pilot[37].

VA-1 did not easily fit any of the aircraft categories for determining flying qualities. As a result, the VA-1 was measured against criteria for class II, medium weight aircraft with low to moderate maneuverability. The reconnaissance portion of the mission would fall under flight phase Category A and the cruise flight condition into

Category B. In general Category A is more restrictive than Category B and for areas where VA-1 met Category A requirements it also met Category B requirements[37].

The parameters used to judge longitudinal flight quality included short period and phugoid damping ratios and the control anticipation parameter (CAP). Parameters used to measure lateral flight quality varied according to the lateral modes: roll, spiral and Dutch roll. Spiral mode was evaluated against a minimum time to double amplitude. Roll mode was measured against a maximum roll time constant. Dutch roll was evaluated with three different criteria: damping ratio, natural frequency and the product of the two[37].

The levels used to quantify the flyability of the aircraft correspond to Cooper-Harper handling qualities scale. Level 1 criteria means the flying quality is satisfactory for the mission flight phase. Level 2 means the flying qualities are acceptable, but either pilot workload is increased or mission performance is degraded with respect to the task, or a combination of the two. Level 3 signifies the need for significant work as it means the pilot workload is considered excessive, mission performance is inadequate or a combination of the two [37]. Any VA-1 configuration meeting level 2 or 3 would need further investigation.

Longitudinal Dynamic Stability

The results show VA-1 has good dynamic stability. Longitudinal flight characteristics were measured against short period and phugoid criteria shown in Table 10. All four configurations had virtually the same short and long period characteristics.

Table 9 shows longitudinal stability parameters for VA-1 with the LVT attached. Phugoid damping ratio was the primary measure for the phugoid mode. Phugoid damping was right at the minimum, 0.04, for level 1 flight quality [37].

Table 9. VA-1 Longitudinal Dynamic Stability.

Mode	Variable of Interest	LVT	Units
Short Period	Damping Ratio, ζ_{sp}	0.85	(-)
	Natural Frequency, ω_n	6.72	(rad/s)
	Control Anticipation Parameter, CAP	3.78	$(1/g/s^2)$
Phugoid	Damping Ratio, ζ	0.04	(-)

Table 10. Longitudinal Flying Qualities[18].

Longitudinal Flying Qualities					
	Short Period				Phugoid
	Categories A and C		Category B		All Categories
Level	ζ_{sp} min	ζ_{sp} max	ζ_{sp} min	ζ_{sp} max	
1	0.35	1.3	0.3	2	ζ>0.04
2	0.25	2	0.2	2	ζ>0
3	0.15	(-)	0.15	(-)	T_2>55 s

VA-1 was stable with respect to the short period mode. Normally the short period mode is examined using the control anticipation parameter, CAP, and short period damping ratio. CAP accounts for how the pilot sitting in the plane senses the aircraft attitude response to a commanded pitch input to change the flight path angle[24]. Since the VA-1 pilot observes the vehicle while standing on the ground, the CAP may not be as important in predicting flying qualities. CAP is commonly used to measure longitudinal

stability, however and is included for comparison value. CAP was defined as $\omega_{n_{sp}}^2 / (n/\alpha)$ for simplicity [26]. The subscripts *sp* denoted short period natural frequency and units were $1/g/s^2$, where *g* was the load factor or g-force. The denominator n/α was found with $n/\alpha = u_1 C_{L_\alpha} QS/g$ where u_1 was the unperturbed freestream velocity in ft/s, C_{L_α} is the aircraft lift curve slope, *Q* is dynamic pressure in lb_f/ft^2, *S* is total wing area in ft^2 and *g* is the gravitational constant[24].

The short period damping ratio, 0.85 for all cases, fell well within the specified range for Level 1 handling in Categories A and B. CAP was compared with specific ranges depending on the short period damping. For a short period damping ration of 0.85 CAP should be between 0.085 and 3.6 for Level 1 in Category B or between 0.28 and 3.6 for Level 1 in Categories A and C. CAP and damping ratio only supported Level 2 for categories A and B as CAP was approximately 3.8, too high for Level 1 but well within the upper limit of 10 for Level 2 [24]. Figure 17 and Figure 18 show how CAP and short period damping together make VA-1 level 2 with respect to this requirement. Once again, VA-1 is unmanned which means CAP requirements do not have the same significance as they would for piloted aircraft. Because CAP does not carry as much weight for this aircraft and the other longitudinal stability parameters show level 1 handling qualities, VA-1 is inherently stable with respect to longitudinal stability. This supports Bowman's prediction of good longitudinal stability[11].

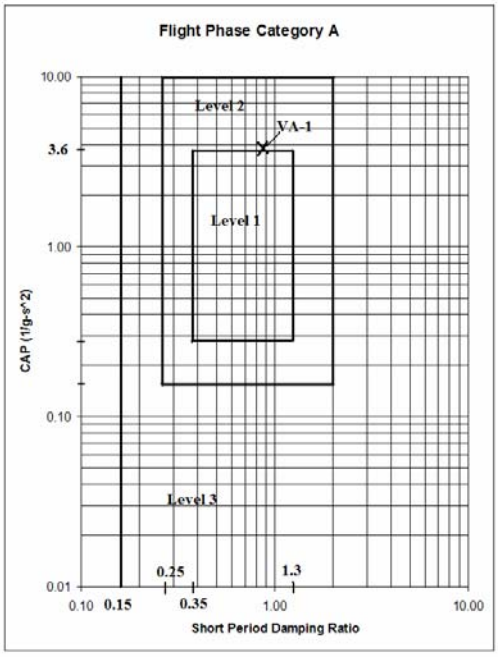

Figure 17. MIL-STD 1797A Criteria for Flight Phase Category A[37].

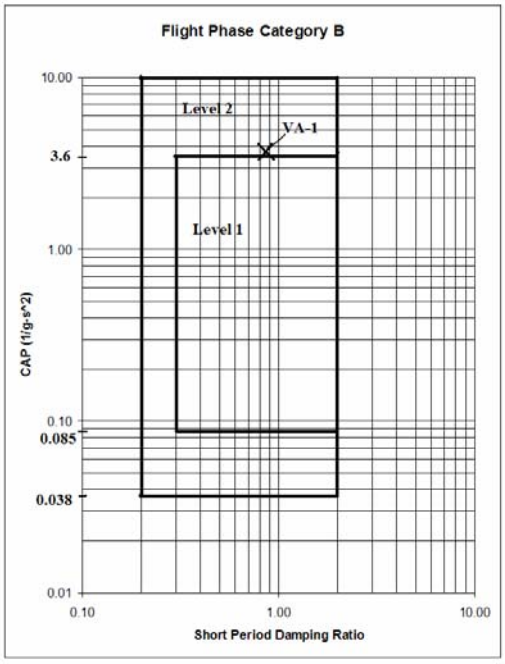

Figure 18. MIL-STD 1797A Criteria for Flight Phase Category B[37].

Lateral Dynamic Stability

All VA-1 configurations met level 1 handling criteria for every lateral mode. Table 11 lists the lateral stability parameters and their associated mode for each configuration. The results for spiral mode will be discussed first, followed by the roll mode and finally Dutch roll.

The spiral mode results disagreed with Bowman's prediction of an unstable spiral mode for the baseline configuration [17]. The spiral mode was stable for the baseline configuration as its eigenvalue had a negative real part. All other configurations had spiral mode eigenvalues with positive real parts and were unstable in the spiral mode.

Table 11 shows the time to double amplitude denoted with an asterisk for configurations with unstable spiral modes: LVT, strutfins and LVT+strutfins. The baseline configuration lists time to half amplitude. Aircraft, however, can be unstable in spiral mode and still meet a level 1 flight quality [18]. Table 12 shows the minimum time to double amplitude for Category A, Level 1 flight qualities is 12 seconds. All configurations exceeded this requirement. In addition the roll mode time constants for all configurations were well below the maximum roll time constant, 1 second, for Level 1, Category A handling[18].

Table 11. VA-1 Lateral Dynamic Stability for Different Configurations.

Mode	Variable of Interest	Baseline	LVT	Strutfins	LVT+ Strutfins	Units
Spiral	Time to Double* or Half Amplitude ,T_d	107.63	61.30*	96.77*	28.69*	(s)
Roll	Time constant , τ	0.05	0.05	0.05	0.05	(s)
Dutch roll	Damping Ratio, ζ	0.22	0.24	0.23	0.25	(-)
	$\zeta\omega_n$	0.62	0.81	0.69	0.88	(rad/s)
	Natural Frequency, ω_n	2.85	3.34	2.94	3.45	(rad/s)

Table 12. MIL-STD 1797A Recommended Spiral Mode Stability[37].

	Minimum Time to Double Amplitude (s)		
Category	Level 1	Level 2	Level 3
A and C	12	8	4
B	20	8	4

Table 13. MIL-STD 1797A Recommended Roll Mode Stability[37].

Roll Mode				
		Maximum Roll Time Constant (s)		
Category	Class	Level 1	Level 2	Level 3
A	I,IV	1	1.4	10
	II,III	1.4	3	10
B	All	1.4	3	10
C	I,II-C,IV	1	1.4	10
	II-L,III	1.4	3	10

Table 14. MIL-STD 1797A Recommended Dutch Roll Stability[37].

Dutch Roll Mode					
Level	Category	Class	**Min ζ** (-)	**Min $\zeta\omega_n$** (rad/s)	**min ω_n** (rad/s)
1	A (CO, GA, RR, TF, RC, FF, AS)	I, II, III, IV	0.4	0.4	1
	A	I, IV	0.19	0.35	1
		II, III	0.19	0.35	0.4
	B	All	0.08	0.15	0.4
	C	I, II-C, IV	0.08	0.15	1
		II-L, III	0.08	0.1	0.4
2	All	All	0.02	0.05	0.4
3	All	All	0	(-)	0.4

The Dutch roll mode also turned out to be stable in cruise, Category B, for all configurations. Table 14 shows the requirements for Dutch roll. Note there are two rows for Category A. The abbreviation RC stands for reconnaissance so the top row was applied. To meet Level 1 Category A for criteria in the Dutch roll mode, the minimum damping allowed was 0.4. The best VA-1 Dutch roll damping is 0.25 for the LVT+strutfins configuration. So for reconnaissance this particular plane is Level 2. For cruise, Category B, however, all configurations easily exceeded the Level 1 requirement.

In conclusion, VA-1 is dynamically stable in cruise flight. This agrees with the flight test video to the degree that erratic flight was not observable for gentle maneuvers. Another important conclusion to be drawn from these results is that VA-1 does not need the LVT or strutfins for stable flight as the baseline configuration meets Level 1 handling qualities for cruise flight in all modes. This means there is opportunity to reduce weight

and drag by removing the LVT. This would reintroduce the problem of protecting the propeller during rotation on takeoff and landing.

One potential solution to that problem would be to place a stiff metal wire in place of the LVT to prevent VA-1 from rotating too far. But cylindrical bodies produce a great deal of drag and this may in fact increase the drag on the aircraft. Another potential solution would be to takeoff without rotating the plane. HASC could be utilized to see if VA-1 can take off with a zero pitch attitude using ailerons and wingtip elevators like flaps. Landing could be accomplished in a similar manner and with the electric motor stopped to protect the propeller.

VII. Preliminary Stall Analysis

Evaluation Method

On its last flight VA-1 landed hard while recovering from what appeared to be a stall that developed in a right hand turn. Before continuing flight tests it is important to know which bank angles are likely to cause a stall and where the stall first occurs. In reality the turn was not likely a true steady state turn, but a steady state level turn will be used to simplify the analysis.

Turn trim conditions, such as control surface deflection and angular rates for roll, pitch and yaw were determined with methods discussed in the trim chapter and put into the HASC input deck. HASC VORLAX output files were used to compute section lift coefficients for the front and rear wings to illustrate a spanwise lift distribution. Sections of the wing that exceeded the two-dimensional airfoil maximum lift coefficient of 1.2 were considered stalled[38]. Three dimensional sections would stall before this point so these computations are only an approximation of the stall. The goal was to find the approximate bank angle where a significant section of the wing might stall and the location of initial stall along the wing.

Section Lift Coefficient

To simplify the spanwise lift distribution results the term section is introduced. HASC uses surfaces, panels and subpanels for bookkeeping. The term section is intended to be a spanwise strip of the forward or rear wing. Some sections were composed of only one panel, while sections with control surfaces were made up of two

panels. The joint was considered its own section. Figure 19 shows the location of each wing section along the right wing. The left wing was divided into similar sections, only in reverse order from root to tip.

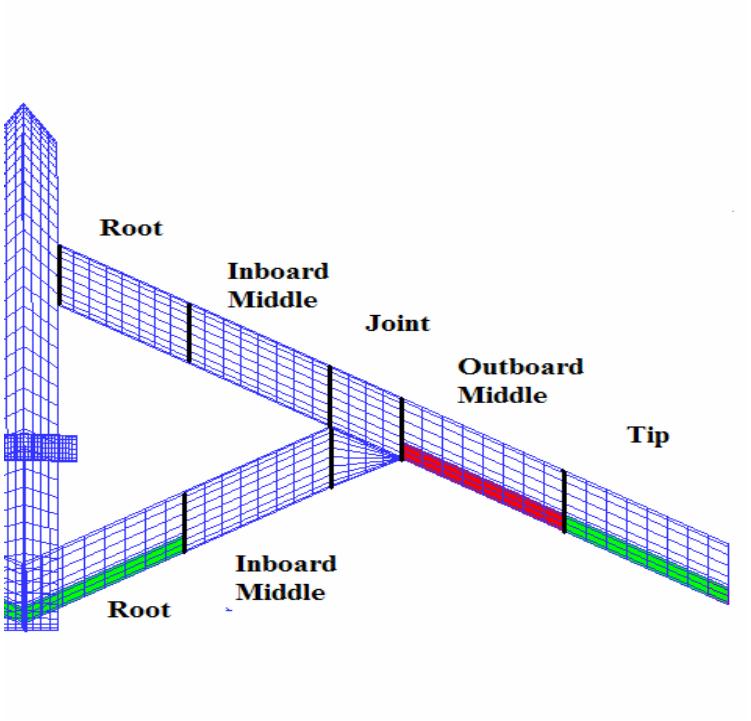

Figure 19. VA-1 Spanwise Wing Sections.

The section lift coefficient was computed for two cases. In the first case the panel area and section area were the same. This method was used for the front wing root and inboard middle sections, as well as the aft wing inboard middle section. The second case required finding the section lift coefficient for sections composed of two panels. The front wing tip and outboard middle sections along with the rear wing root fell into this category. The equation for the case where the panel area equals the section area is discussed first.

The VORLAX output from HASC tabulated the local lift coefficient for each panel, non-dimensionalized using total wing area. Each panel lift coefficient could then be summed together to find the total lift coefficient for the complete aircraft. The equation for panel lift coefficient would be $C_{L_i} = L_i / QS$ where L_i is the panel lift in lb_f, Q is the dynamic pressure in lb_f/ft^2 and S is the total wing reference area in ft^2. The subscript i represents the panel number. For this analysis local lift coefficient with respect to the section area is desired instead of the coefficients direct from VORLAX.

The equation for section lift coefficient is then $C_{L_{section}} = L_{section} / QS_{section}$ where $L_{section}$ is the lift and $S_{section}$ is the area for the respective wing section. For wing sections composed of one panel, $L_i = L_{section}$ and $S_i = S_{section}$. To convert the panel lift coefficient to section lift coefficient, the panel lift coefficient was divided by the panel surface area, S_i, and multiplied by total area, S:

$$C_{L_{section}} = C_{L_i} \frac{S}{S_i} \tag{7}$$

Were $S/S_i = S/S_{section}$.

The calculation differed for sections composed of two panels. For example, the wing tip section is composed of two panels: a trailing edge device and an adjacent upstream panel. For illustration purposes, let's assign trailing edge device and the adjacent upstream panels to i = 1 and 2 respectively. First add the lift coefficients, non-dimensionalized with total wing area, together to get $C_{L_1} + C_{L_2} = (L_1 + L_2)/(QS)$. Then multiply both sides by $S/(S_1+S_2)$ to end up with the equation used to find the section lift coefficient for sections with two panels:

$$C_{L_{section}} = \frac{\left(C_{L_1} + C_{L_2}\right)S}{\left(S_1 + S_2\right)} \tag{8}$$

which is equivalent to $(L_1+L_2)/(Q(S_1+S_2))$ or $L_{section}/QS_{section}$. With equations for sections with one and two panels respectively, a spanwise lift coefficient distribution was created.

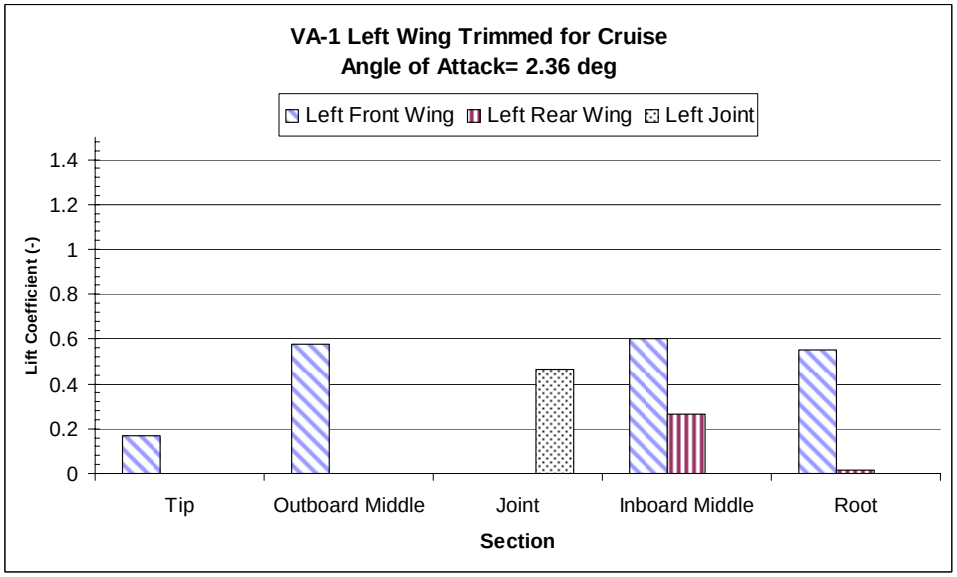

Figure 20. VA-1 Left Wing Lift Coefficient Distribution for Straight and Level Flight.

Figure 20 shows the lift coefficients for each spanwise section when VA-1 is trimmed for straight and level flight. In straight and level flight the right wing lift coefficient distribution mirrors the left. Figure 21 and Figure 22 show the section lift coefficients for the left and right wings respectively when VA-1 is trimmed for level right hand turn with 50 degrees of bank. The outboard middle section on the left front wing approaches stall first. Figure 23 and Figure 24 show the outboard middle section on the

left wing exceeds the airfoil's maximum lift coefficient and potentially stalls at 55 degrees of bank.

The results make sense as the ailerons were located at the outboard middle wing sections. In a right had turn the left aileron is deflected trailing edge down to increase the local lift coefficient and effect the turn. The aileron on the right wing is deflected trailing edge up so that the aileron section inside the turn reduces the local lift. Thus it makes sense that the right wing does not approach stall before the left wing in a trimmed right hand level turn. The relatively lower lift coefficients for the front wing tips and rear wing roots were partly due to the fact that these sections included elevator control sections. During the bank all elevator control surfaces were moved trailing edge up, reducing the local lift for each rear wing root and front wing tip section.

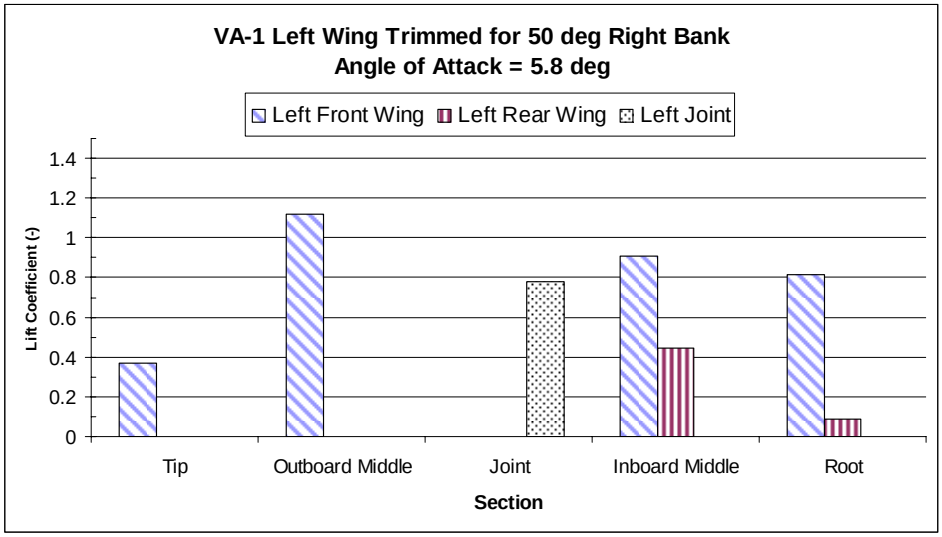

Figure 21. VA-1 Left Wing with 50 Degree Bank Angle.

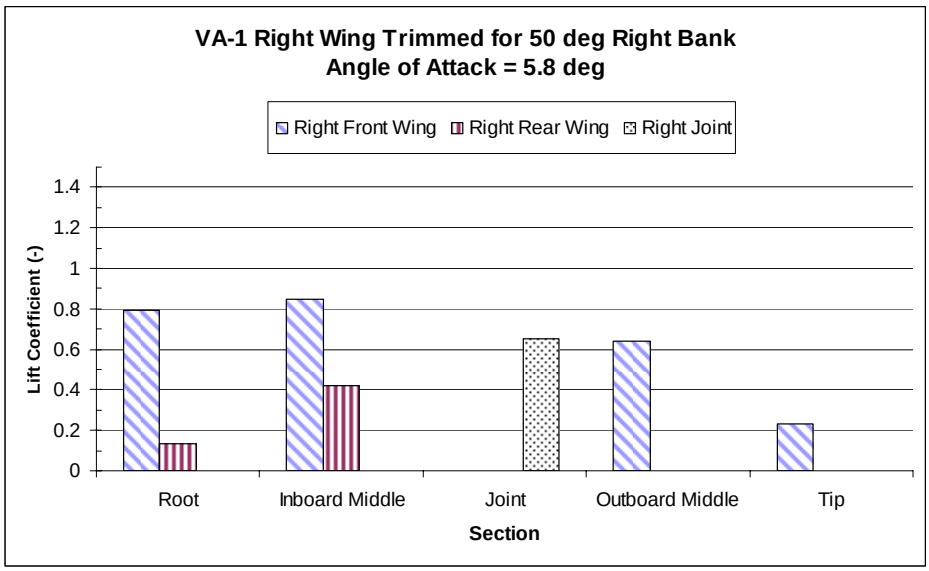

Figure 22. VA-1 Right Wing with 50 Degree Bank Angle.

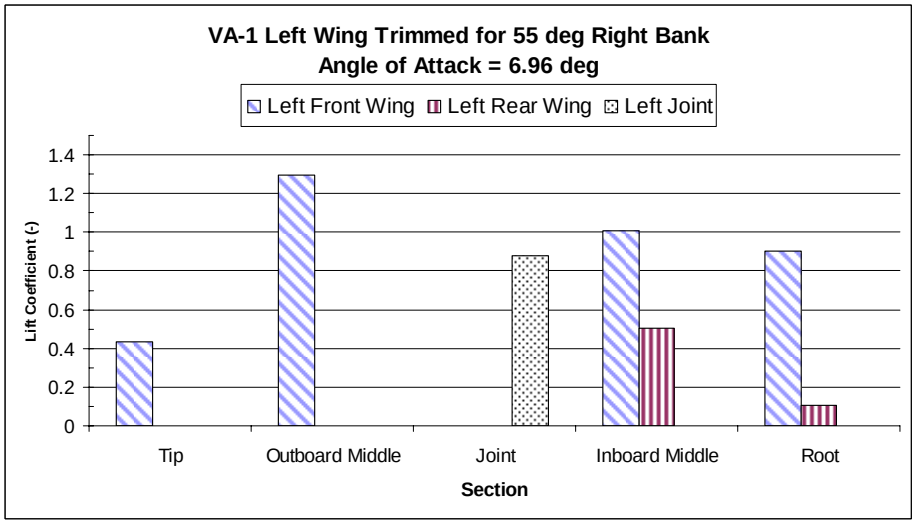

Figure 23. VA-1 Left Wing with 55 Degree Bank Angle.

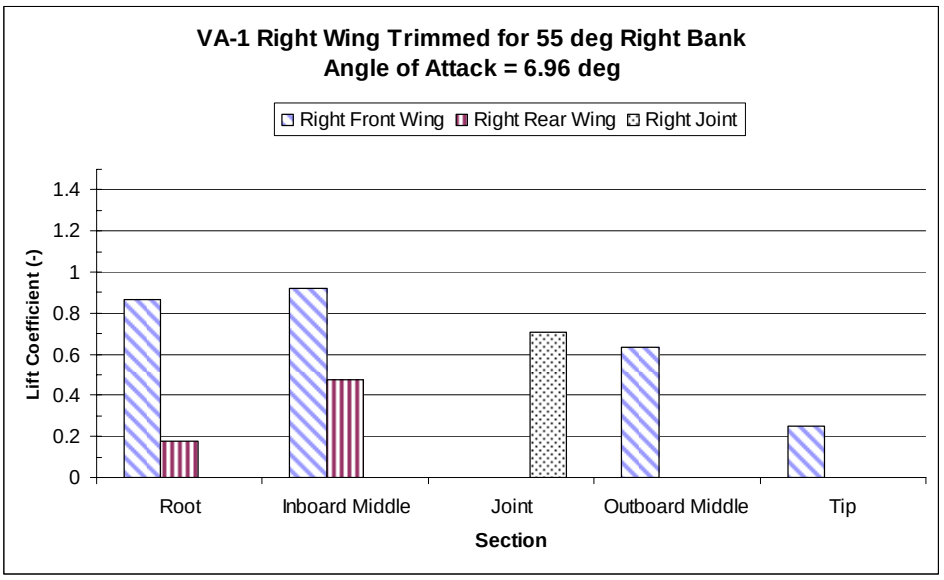

Figure 24. VA-1 Right Wing with 55 Degree Bank Angle.

These results do not agree the flight test video which showed the inboard wing buffet, suggesting the wing inside the turn stalled first. The difference was possibly due to a combined turn and descent. For turns coupled with a change in altitude the roll rate is no longer zero. On a descending right turn aircraft rolls into the turn, rolling right wing down. This roll rate causes a local increase in the effective angle of attack on the inside wing, which could contribute to an inside wing stall[34]. To explore this effect a 20 deg/s right roll rate was added to HASC input deck trimmed for a steady level 50 degree right hand turn was given to see the effective change in angle of attack on the wings in the descending turn. This was not enough for any inside wing sections to stall, but several right wing panels increased in lift coefficient by approximately 0.1 suggesting an increase in local angle of attack.

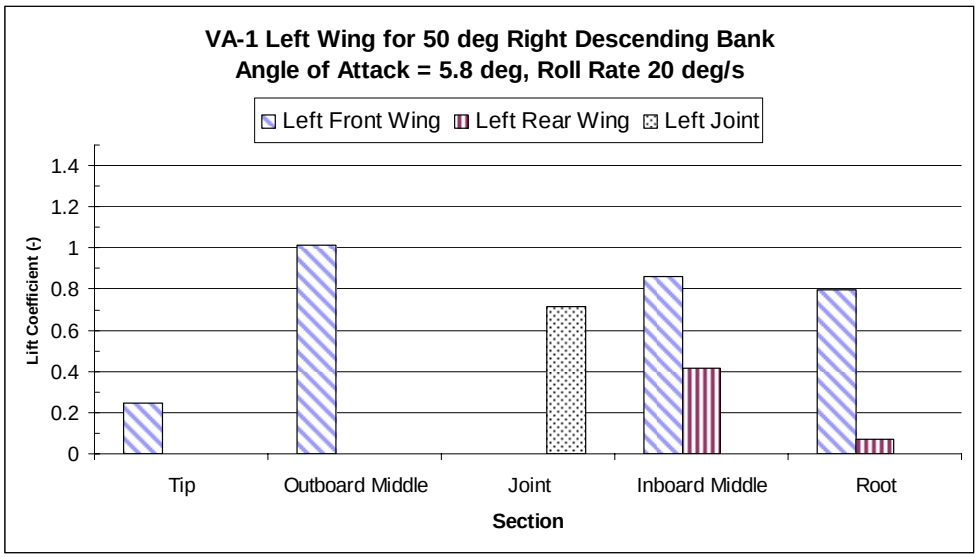

Figure 25. VA-1 Left Wing with 50 Degree Bank Angle and 20 deg/s Roll Rate.

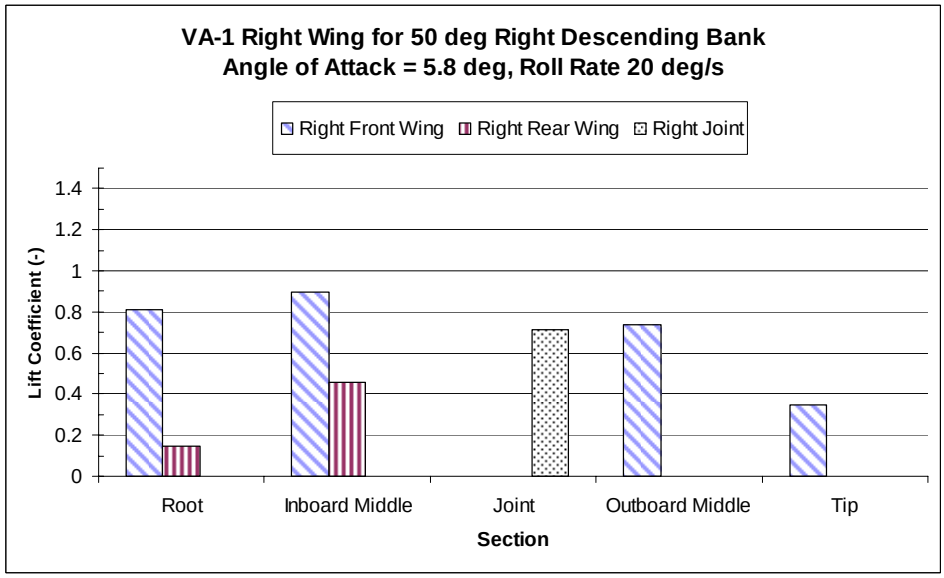

Figure 26. VA-1 Right Wing with 50 Degree Bank Angle and 20 deg/s Roll Rate.

For trimmed level turning flight, the stall occurs between 50 and 55 degrees of bank. In this case, stall appears to begin at the outboard middle section of the wing outside the turn. In general when the wing outside the turn stalls first, recovery is relatively easy as the aircraft would simply roll itself out of the turn. Since the pilot does not have a real time bank angle indicator from which to read bank angle a good rule of thumb for future flight tests might be to avoid banking more than 45 degrees when possible. The 45 degree bank angle limitation also provides some margin for error as distance and viewing angle would make judging 45 degrees of bank difficult.

Wing tip stall is typically avoided to preserve aileron effectiveness, which aids stall recovery by preventing loss of aircraft control. In the turning maneuver, stall first occurs inboard of the tip. Unfortunately this is still where the aileron is located. Some standard procedures to prevent stall over the ailerons would be geometrically twisting the wing section or adding a leading edge slot or slat to increase the stall angle of attack for the aileron portion of the wing[23].

For descending turns the inside wing can stall first, especially if the airspeed is low in the turn. Recovering from the condition where the wing inside the turn stalls is more difficult because the turn quickly becomes steeper due to loss of lift on the inside wing, and the airplane may enter a spiral dive[34]. This complicates recovery as the aircraft loses altitude quickly and may have lost control surface effectiveness needed to recover. Clearly the inside wing in the turn stalling is the more severe condition. More research should be done with regard to how to predict stall in descending turns.

VIII. Conclusions and Recommendations

Conclusions of Research

The inertia twist test was a simple low technology method for measuring the inertia about the roll, pitch and yaw axes. VA-1 inertia was found to be near 3-5 slug-ft^2 about the roll, pitch and yaw body axes. Secondary oscillations appeared to affect the results only slightly but left room for test design improvement. The roll test moved the wings normal to the air and exhibited visible signs of damping. The estimated damping for the roll test, based on the logarithmic decrement, was accounted for in the results. A release mechanism would be useful for reducing wobble introduced by the testers as they released the airplane from its initial position. Future inertia tests may be simplified, when possible, by suspending the aircraft from a structure that is closer to the ground.

VA-1, despite its unusual joined-wing geometry, is dynamically stable in cruise flight. This agrees with the flight test video to the degree that erratic flight was not observable for gentle maneuvers[36]. Wind tunnel tests could not support this conclusion in the same manner as the vehicle would need to be constrained in some manner. The analysis also revealed VA-1 was stable enough to remove the LVT without significant loss of stability. This would reduce weight and drag in the event of any future flights. Finally, dynamic instability in the cruise flight condition was not a likely contributing factor to the hard landing in October of 2005.

A simple examination of the wing spanwise lift coefficient distribution revealed VA-1 could perform a trimmed bank up to 50 degrees without stalling. For trimmed turns the aileron on the outside wing approaches stall first. A descending turn was also

briefly considered. Adding a roll rate to the HASC model demonstrated that HASC has the potential to model the change in lift distribution due to a descending turn. Additional research would be required to find more realistic flight conditions for analyzing a descending turn in HASC.

HASC was found to be a flexible tool for computing aerodynamic forces and moment coefficients and non-dimensional stability derivatives. Unusual control surface combinations could also be analyzed. HASC was also useful for computing the change in downwash with respect to change in angle of attack, which was used to find a stability derivative needed for the dynamic stability model. The HASC VORLAX output became a useful tool for examining the spanwise lift coefficient distribution along the wings. This allowed a preliminary analysis of the spanwise lift distribution across the wings

Significance of Research

This research contributed to AFRL research regarding a promising UAV reconnaissance platform. The unique joined-wing aircraft geometry has the potential to carry a highly effective antenna array with 360 degree coverage and improved ability to penetrate dense foliage. Specifically, this research was the first to quantify flight handling qualities for VA-1, a joined-wing flight demonstrator. Stability derivatives for VA-1 in four different configurations were evaluated. Experimentally measured inertia data from this research may be used for any future dynamic stability studies of this joined-wing configuration. The preliminary stall analysis method may be used to gain insight into stall phenomena in descending turns. On a final note, this model neglected a key design issue for high altitude joined-wing aircraft: aeroelasticity. Some of the basic

methods used in this study could, however, be expanded to model aeroelastic effects in future flight quality studies for joined-wing aircraft.

Recommendations for Action

The LVT was not critical for dynamic stability in cruise flight. Removing the surface would save weight and reduce drag. But then there is no protection for the propeller during takeoff rotation. HASC could be utilized to see if VA-1 can take off with a zero pitch attitude using ailerons and wingtip elevators like flaps. Stopping the electric engine during landing could be a method protect the propeller at the end of flight.

Research is recommended to determine if the potential pitch-up instability near stall angles of attack found on JW-1 would occur on VA-1. This fell outside the scope of this analysis, but may be of concern for future joined-wing research. A potential means to fix this problem could be adjusting the wing twist distribution.

More research is recommended to evaluate potential stall on the inside wing in descending turns. A useful outcome of such research could be a recommended stall speed for descending turns. Adding washout to the wing outside the joint would reduce the local angle of attack and may reduce the tendency for the wing inside the turn to stall during slow descending turns.

Summary

Predicting the dynamic stability for VA-1 required a great deal of information obtained from different methods. In order to analyze dynamic stability, the inertia about the three body axes was experimentally measured using a twist test. A VLM program

called HASC-95 was used to determine the non-dimensional aerodynamic force and moment coefficients for VA-1. Non-dimensional stability derivatives for the baseline, LVT, strutfin and LVT+strutfin configurations were computed. These stability derivatives and aircraft inertias were used in the longitudinal and lateral stability models. The stability criteria for each of the longitudinal and lateral modes were evaluated against to flight handling qualities criteria outlined in MIL-STD 1797A and common aircraft stability and control texts. VA-1 was found to have good longitudinal and lateral flying qualities in cruise flight.

A preliminary stall analysis for turning flight was conducted with HASC. VA-1 was found to be capable of trimmed level turns of up to 50 degrees of bank with an acceptable stall margin. More research should be done regarding stall on the inside wing during descending turns.

Appendix A: Twist Test Equation Derivation and Uncertainty Analysis

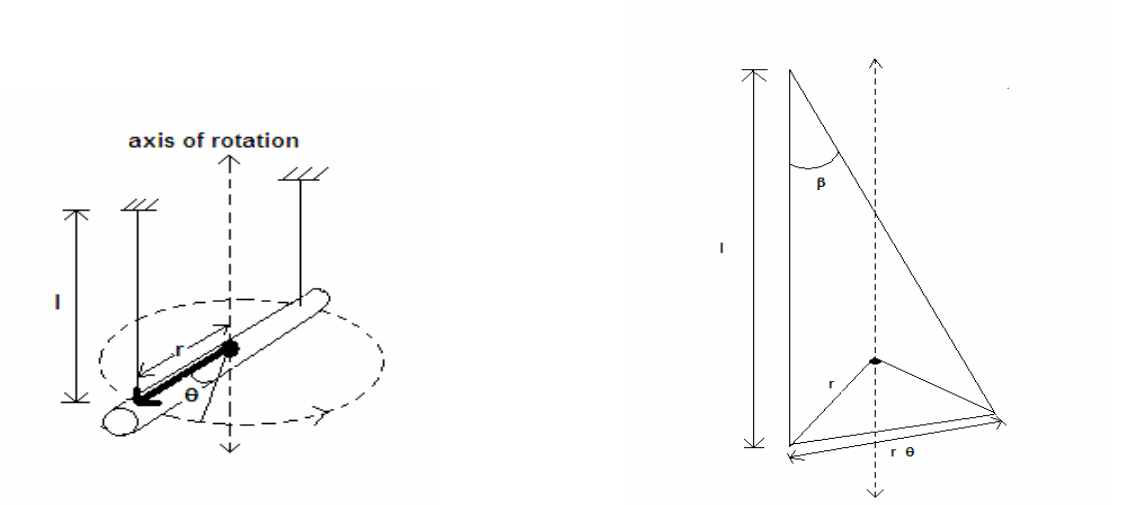

Fig A1. Twist test for a cylinder

Assume a cylindrical bar of uniform density is suspended by two cords of equal length. The dashed line passes through the bar's center of mass and represents the axis about which the mass moment of inertia is to be measured. The bar is twisted θ radians from it equilibrium position and released. Assuming no external forces act on the bar after release an expression will be derived to find Inertia as a function of the period, *P*. Assuming each cord is exactly the same length and that the weight is distributed evenly between them so that the tension, *T*, in each chord is ½ *W*. The horizontal component of tension for one cord can be expressed by:

$$T_h = \tfrac{1}{2} W \sin \beta$$

where

T_h = horizontal component of tension

β = angle between vertical and cable (rad)

W = weight (lb_f)

The attachment point follows a circular path. Assuming small angles however, the distance can be estimated using the following relationship:

$$\sin\beta = \frac{r\theta}{l}$$

where

l = cable length (ft)

r = distance from bar c.g. to attachment point (ft)

θ = angular rotation in horizontal plane (rad)

By substitution the horizontal tension can be calculated from:

$$T_h = \frac{1}{2} W \frac{r\theta}{l}$$

Sum of the moments about the center of rotation yields the key equation:

$$\sum M = I\ddot{\theta}$$

where

M = moments ($ft\text{-}lb_f$)

I = Inertia ($slug\text{-}ft^2$)

The sum of the moments are equal to the total horizontal tension times radius of rotation:

$$-2T_h r = I\ddot{\theta}$$

Substitute for horizontal tension:

$$-2\left(\frac{1}{2}W\frac{r\theta}{l}\right)r = I\ddot{\theta}$$

Set equal to zero and solve for the second order ordinary differential equation:

$$I\ddot{\theta} + \frac{Wr^2}{l}\theta = 0$$

Divide through by inertia term

$$\ddot{\theta} + \frac{Wr^2}{I\,l}\theta = 0$$

Note the differential equation of the following form:

$$\ddot{\theta} + \omega_n{}^2\theta = 0$$

Solving for natural frequency, ω_n, in units of 1/sec

$$\omega_n{}^2 = \frac{Wr^2}{I\,l}$$

$$\omega_n = r\sqrt{\frac{W}{I\,l}}$$

The period, P, in seconds is related to the natural frequency with the following:

$$P = \frac{2\pi}{\omega_n} = \frac{2\pi}{r\sqrt{\frac{W}{I\,l}}}$$

Solving for Inertia as a function of the period, weight, cable length and radius of rotation:

$$\sqrt{\frac{W}{I\,l}} = \frac{2\pi}{rP}$$

$$\frac{W}{I\,l} = \frac{4\pi^2}{r^2 P^2}$$

The following equation can be used to find the inertia:

$$I = \frac{W}{l}\frac{r^2 P^2}{4\pi^2}$$

To increase the accuracy of the experiment, the distance, *d*, between the cords was used were $r=d/2$. By substitution the inertia is $I = (Wd^2P^2)/(16\pi^2 l)$.

Uncertainty Analysis

To ensure numerical accuracy of the results an uncertainty analysis was conducted. First, the partial derivatives of *I* with respect to the variables *W*, *r*, *P* and *l* was determined. The δ notation signifies the uncertainty for each measurement. For example, δr was the uncertainty of the radius of rotation and was estimated to be +/- in. The equation for δI is the basic equation for uncertainty in the inertia calculation.

$$\frac{\partial I}{\partial W} = \frac{r^2 P^2}{4\pi^2 l}$$

$$\frac{\partial I}{\partial r} = 2\frac{WrP^2}{4\pi^2 l}$$

$$\frac{\partial I}{\partial P} = 2\frac{Wr^2 P}{4\pi^2 l}$$

$$\frac{\partial I}{\partial l} = -\frac{Wr^2P^2}{4\pi^2 l^2}$$

$$\delta I = \sqrt{\left(\frac{\partial I}{\partial W}\delta W\right)^2 + \left(\frac{\partial I}{\partial r}\delta r\right)^2 + \left(\frac{\partial I}{\partial P}\delta P\right)^2 + \left(\frac{\partial I}{\partial l}\delta l\right)^2}$$

Appendix B: Wortmann FX 60-100 Airfoil Data

This data came from the Nihon University Aeronautical Student Group (NASG) web based database.

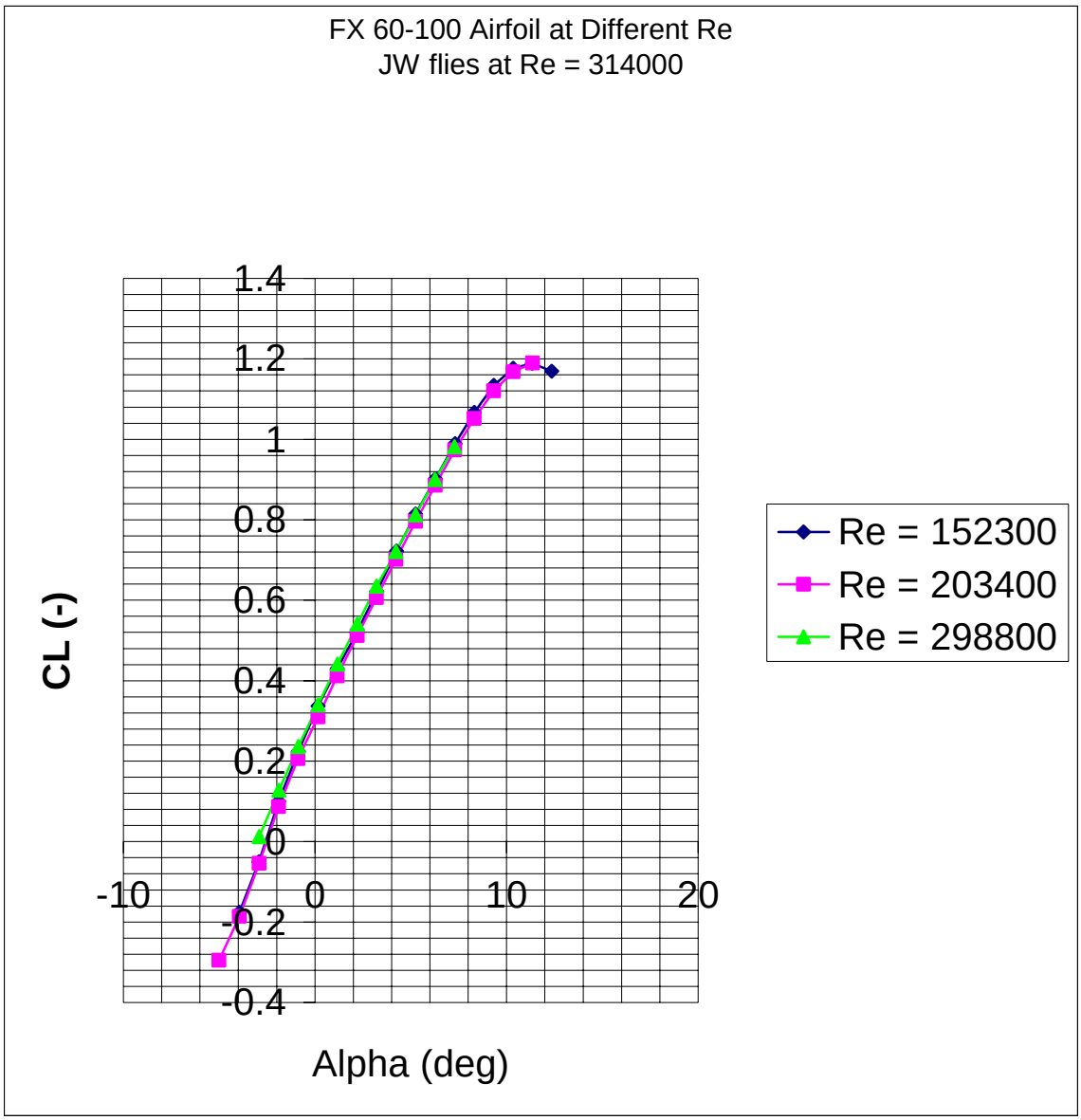

Bibliography

1. Miller, M.P. An Accurate Method of Measuring the Moments of Inertia of Airplanes. Technical notes National Advisory Committee for Aeronautics (NACA) Report No. 351. Washington: Langley Memorial Aeronautical Laboratory, 1930.

2. Wolkovitch, J. *Joined Wing Aircraft*, US Patent 3,942,747, March 1976.

3. Samuels, M. F., "Structural Weight Comparison of a Joined Wing and a Conventional Wing," *Journal of Aircraft*, Vol. 19, No. 6, 1982, pp.485-491.

4. Wolkovitch, J., "The Joined Wing: An Overview," *Journal of Aircraft*, 23:161-178 (March 1986).

5. Smith, S. C., Cliff S.E., and Kroo, I.M., "The Design of a Joined-Wing Flight Demonstrator Aircraft", AIAA Paper 87-2930, AIAA/AHS/ASEE Aircraft Design, Systems and Operations Meeting, St. Louis, MO, 14-16 September 1987.

6. Gallman, J.W., Kroo, I.M., and Smith, S.C. "Design Synthesis and optimization of Joined-Wing Transports", AIAA-90-3197, presented at the AIAA/AHS/ASEE Aircraft Design, Systems and Operations Meeting, Dayton, OH, 17-19 September 1990.

7. Kroo, I. M., Gallman, J.W., and Smith, S.C. "Aerodynamic and Structural Studies of Joined-Wing Aircraft." *Journal of Aircraft*, Vol. 28, No.1, January-February 1991, pp. 74-81.

8. Reich, G.W., Raveh, D., and Zink, P.S. "Application of Active Aeroelastic Wing Technology to a Joined-Wing SensorCraft", AIAA-1001-1633, presented at the 43rd AIAA/ASME/ASCE/AHS/ASC Structures, Structural Dynamics, and Materials Conference, Denver, CO, 22-25 April 2002.

9. Nangia, R.K., "Towards Designing Novel High Altitude Joined-Wing Sensor-Craft (HALE-UAV)", AIAA-2003-2695, presented at the AIAA/ICAS International Air & Space Symposium, Dayton, OH, 14-17 July 2003.

10. Roberts, Ronald. *Sensor-Craft Analytical Certification*, MS Thesis, Graduate School of Engineering, Air Force Institute of Technology (AETC), Wright-Patterson AFB, Ohio, March 2003. AFIT/GAE/ENY/03-06.

11. Bowman, Jason. "Stability and Control Analysis of the AFRL Radio-Controlled Joined Wing." Report to AFRL/VA personnel, WPAFB, Ohio, 2003.

12. Smallwood, B. *Structurally Integrated Antennas on a Joined-Wing Aircraft.* MS Thesis, Graduate School of Engineering, Air Force Institute of Technology (AETC), Wright-Patterson AFB OH, March 2003. AFIT/GAE/ENY/03-07.

13. Sitz, J.J., *Aeroelastic Analysis of a Joined Wing Sensorcraft.* MS Thesis, Graduate School of Engineering, Air Force Institute of Technology (AETC), Wright-Patterson AFB, Ohio, March 2004. AFT/GAE/ENY/04-J12.

14. Rasmussen C.C., *Optimization Process for Configuration of a Flexible Joined-Wing.* MS Thesis, Graduate School of Engineering, Air Force Institute of Technology (AETC), Wright-Patterson AFB, Ohio, March 2004. AFT/GAE/ENY/04-M14.

15. Nangia, R.K., Palmer, M.E., and Tilmann, C.P., "Planform Variation Effects in Unconventional High Aspect Ratio Joined-Wing Aircraft Incorporating Laminar Flow", AIAA-2005-0243, presented at the 42nd AIAA Aerospace Sciences Meeting and Exhibit, Reno, NV, 10-13 January 2005.

16. Craft, Ryan L., *Drag Estimates for the Joined-Wing Sensorcraft.* MS Thesis, Graduate School of Engineering, Air Force Institute of Technology (AETC), Wright-Patterson AFB, Ohio, March 2005. AFT/GAE/ENY/05-J02.

17. Raymer, Daniel P. Aircraft Design: A Conceptual Approach (2nd Edition). Washington DC: American Institute of Aeronautics and Astronautics, Inc., 1992.

18. Nelson, R. *Flight Stability and Automatic Control* (2nd Edition). Boston, McGraw Hill, 1998.

19. Althaus, Dieter and Wortmann, F.X. *Stuttgarter Profilkatalog I.* Braunschweig, Friedr. Vieweg & Sohnn, 1981.

20. *High Angle of Attack Stability and Control 95*. (HASC95) Computer Software. NASA Langley Research Center, 1995.

21. Albright, Alan E., Dixon, Charles J., Hegedus, Martin C. "Modification and Validation of Conceptual Design Aerodynamic Prediction Method HASC95 with VTXCHN."

22. Riley, William F., Sturges, Leroy D. *Engineering Mechanics: Dynamics (2nd Edition).* New York, John Wiley and Sons, Inc., 1996.

23. Bertin, John J. Aerodynamics for Engineers (4th Edition). New Jersey, Prentice Hall, 2002.

24. Roskam, Jan. Airplane Flight Dynamics and Automatic Flight Controls: Part I. Lawrence, Design, Analysis and Research Corporation, 1995.

25. Stevens, Brian L., Lewis, Frank L. Aircraft Control and Simulation. (2nd Edition). Hoboken, John Wiley and Sons, Inc., 2003.

26. Department of Defense. Military Standard Flying Qualities of Piloted Aircraft. MIL-STD-1797A, Washington: Government Printing Office, 30 Jan 1990.

27. "MATLAB Version 7.1.0.246(R14) Service Pack (3)," The Mathworks, Inc. 2005.

28. Roskam, Jan. Airplane Design: Part VI: Preliminary Calculations of Aerodynamic, Thrust and Power Characteristics. Lawrence, KS, 1990.

29. Blair, M. "Technical Review Board: Joined-Wing Technology Demonstrator." Briefing to AFRL/Personnel, WPAFB, OH, May 2004.

30. Blair, M., Canfield, R., Roberts R. W. Jr., "Joined-Wing Aeroelastic Design with Geometric Nonlinearity." *Journal of Aircraft*, Vol. 42, No.4, August 2005, pp. 832-848.

31. Bowman, J. "Cruise Velocity Analysis." Report to AFRL/VA personnel, WPAFB, Ohio, 2003.

32. Hodgkinson, J. "Aircraft Handling Qualities." Reston, VA, Blackwell Science Ltd., 1999.

33. Meirovitch, L. "Fundamentals of Vibrations." New York, NY, McGraw-Hill, 2001.

34. Stinton, D. "Flying Qualities and Flight Testing of the Airplane." Reston, VA, American Institute of Aeronautics and Astronautics, 1996.

35. Roskam, J. "Airplane Design Part IV: Preliminary Calculation of Aerodynamic, Thrust and Power Characteristics." Ottowa, KS, 1990.

36. "Joined-Wing." VA-1 Flight Test Database. Version 1.0. CD-ROM. AFRL/VACA: WPAFB Ohio, 2005.

37. Yechout, T. R. "Introduction to Aircraft Flight Mechanics: Performance, Static Stability, Dynamic Stability, and Classical Feedback Control." Reston, VA, American Institute of Aeronautics and Astronautics, 2003.

38. Takeuchi, H. "Wortmann FX 60-100 airfoil." From Nihon University Aeronautical Student Group (NASG) database. n. pag. http://www.nasg.com/afdb/show-airfoil-e.phtml?id=291, 1 Dec 2005.

Vita

Capt William A. McClelland graduated from Joseph Wheeler High School in Marietta, Georgia. He entered undergraduate studies at the United States Air Force Academy in Colorado Springs, Colorado where he graduated with a Bachelor of Science degree in Aeronautical Engineering in June 1999. He was commissioned into the Air Force on 2 Jun 99.

His first assignment was at Vandenberg AFB as a student in Undergraduate Space and Missile training in August 1999. In April 2000 he was assigned to the 741st Missile Squadron, Minot AFB, North Dakota were he served as an ICBM combat crew officer. In August 2004, he entered the Graduate School of Engineering and Management, Air Force Institute of Technology. Upon graduation he will be assigned to the Air Force Research Laboratory at Wright-Patterson Air Force Base.

REPORT DOCUMENTATION PAGE

Form Approved
OMB No. 074-0188

The public reporting burden for this collection of information is estimated to average 1 hour per response, including the time for reviewing instructions, searching existing data sources, gathering and maintaining the data needed, and completing and reviewing the collection of information. Send comments regarding this burden estimate or any other aspect of the collection of information, including suggestions for reducing this burden to Department of Defense, Washington Headquarters Services, Directorate for Information Operations and Reports (0704-0188), 1215 Jefferson Davis Highway, Suite 1204, Arlington, VA 22202-4302. Respondents should be aware that notwithstanding any other provision of law, no person shall be subject to an penalty for failing to comply with a collection of information if it does not display a currently valid OMB control number.
PLEASE DO NOT RETURN YOUR FORM TO THE ABOVE ADDRESS.

1. REPORT DATE *(DD-MM-YYYY)*	**2. REPORT TYPE**	**3. DATES COVERED** *(From – To)*
23-03-2006	Master's Thesis	March 2005 – March 2006

4. TITLE AND SUBTITLE

Inertia Measurement And Dynamic Stability Analysis Of A Radio-Controlled Joined-Wing Aircraft

5a. CONTRACT NUMBER

5b. GRANT NUMBER

5c. PROGRAM ELEMENT NUMBER

6. AUTHOR(S)

McClelland, William A., Captain, USAF

5d. PROJECT NUMBER

5e. TASK NUMBER

5f. WORK UNIT NUMBER

7. PERFORMING ORGANIZATION NAMES(S) AND ADDRESS(S)
Air Force Institute of Technology
Graduate School of Engineering and Management (AFIT/EN)
2950 Hobson Way, Building 640
WPAFB OH 45433-8865

8. PERFORMING ORGANIZATION REPORT NUMBER

AFIT/GA/ENY/06-M07

9. SPONSORING/MONITORING AGENCY NAME(S) AND ADDRESS(ES)
Air Force Research Laboratory/VASD
Attn: Dr. Maxwell Blair
2130 Eighth Street, Bldg 146
WPAFB OH 45433-7542 DSN: 785-8430

10. SPONSOR/MONITOR'S ACRONYM(S)

11. SPONSOR/MONITOR'S REPORT NUMBER(S)

12. DISTRIBUTION/AVAILABILITY STATEMENT

APPROVED FOR PUBLIC RELEASE; DISTRIBUTION UNLIMITED.

13. SUPPLEMENTARY NOTES

14. ABSTRACT

Dynamic stability and stall during steady level turns were examined for VA-1, a joined-wing flight demonstrator aircraft. Configurations with a lower vertical tail and fairings over the main landing gear were compared with a recommendation on the combination had the best drag and dynamic stability characteristics. The dynamic stability analysis was broken into four key parts: a twist test experimentally measured mass moments of inertia, a panel method was used to find non-dimensional stability derivatives, lateral and longitudinal state space models estimated dynamic stability characteristics and handling quality levels were evaluated using a Cooper-Harper based rating system. VA-1 was found to have good longitudinal and lateral flight qualities for cruise flight. The lower vertical tail could be removed to reduce weight and drag without degrading dynamic stability. Spanwise lift coefficients for different wing sections in trimmed steady state turns at 50 and 55 degrees of bank were estimated to see which sections of the wing stalled first. The analysis revealed VA-1 can turn using bank angles less than 50 degrees without stall and that stall first occurred at the aileron, immediately outboard of the wing joint.

15. SUBJECT TERMS
Joined-wing, vortex lattice method, aerodynamic stability, flight testing, stalling, HASC, trim(aerodynamics)

16. SECURITY CLASSIFICATION OF:			**17. LIMITATION OF ABSTRACT**	**18. NUMBER OF PAGES**	**19a. NAME OF RESPONSIBLE PERSON**
a. REPORT	**b. ABSTRACT**	**c. THIS PAGE**			Robert A. Canfield
U	**U**	**U**	**UU**	102	**19b. TELEPHONE NUMBER** *(Include area code)* (937) 255-6565, ext 4723 (emailname@afit.edu)

Standard Form 298 (Rev. 8-98)
Prescribed by ANSI Std. Z39-18